Performance Analysis of mmWave Radio Propagations in an Indoor Environment for 5G Networks

Hanna Getahun

A Thesis Submitted to

The Department of Electronics and Communication Engineering

School of Electrical Engineering and Computing

Presented in Partial Fulfillment of the Requirement for the Degree of Master's in Electronics and Communication Engineering (Communication Engineering)

Office of Graduate Studies

Adama Science and Technology University

September, 2021

Adama, Ethiopia

Performance Analysis of mmWave Radio Propagations in an Indoor Environment for 5G Networks

Hanna Getahun

Advisor: Dr. Rajkumar S (PhD)

Co-Advisor: Mr. Shanko Chura

A Thesis Submitted to
The Department of Electronics and Communication Engineering
School of Electrical Engineering and Computing

Presented in Partial Fulfillment of the Requirement for the Degree of Master's in Electronics and Communication Engineering (Communication Engineering)

Office of Graduate Studies
Adama Science and Technology University

September, 2021

Adama, Ethiopia

DECLARATION

I hereby declare that this Master Thesis entitled "Performance Analysis of mmWave Radio Propagations in an indoor environment for 5G Networks" is my original work. That is, it has not been submitted for the award of any academic degree, diploma or certificate in any other university. All sources of materials that are used for this thesis have been duly acknowledged through citations.

______________________	______________________	______________
Name of the student	Signature	Date

RECOMMENDATION

We, the advisors of this thesis, hereby certify that we have read the revised version of the thesis entitled “Performance Analysis of mmWave Radio Propagations in an indoor environment for 5G Networks” prepared under our guidance by Hanna Getahun submitted in partial fulfillment of the requirements for the degree of Mater’s of Science in Electronics and Communication Engineering (Communication Engineering). Therefore, we recommend the submission of revised version of the thesis to the department following the applicable procedures.

______________________	______________________	______________
Major Advisor	Signature	Date
______________________	______________________	______________
Co-advisor	Signature	Date

APPROVAL PAGE OF M.SC. THESIS

We, the advisors of the thesis entitled "Performance Analysis of mmWave Radio Propagations in an indoor environment for 5G Networks" and developed by Hanna Getahun, hereby certify that the recommendation and suggestions made by the board of examiners are appropriately incorporated into the final version of the thesis.

______________________	______________________	______________
Major Advisor	Signature	Date
______________________	______________________	______________
Co-advisor	Signature	Date

We, the undersigned, members of the Board of Examiners of the thesis by Hanna Getahun have read and evaluated the thesis entitled "Performance Analysis of mmWave Radio Propagations in an indoor environment for 5G Networks" and examined the candidate during open defense. This is, therefore, to certify that the thesis is accepted for partial fulfillment of the requirement of the degree of Master of Science in Electronics and Communication engineering (Communication Engineering).

______________________	______________________	______________
Chairperson	Signature	Date
______________________	______________________	______________
Internal Examiner	Signature	Date
______________________	______________________	______________
Eternal Examiner	Signature	Date

Finally, approval and acceptance of the thesis is contingent upon submission of its final copy to the Office of Postgraduate Studies (OPGS) through the Department Graduate Council (DGC) and School Graduate Committee (SGC).

______________________	______________________	______________
Department Head	Signature	Date
______________________	______________________	______________
School Dean	Signature	Date
______________________	______________________	______________
Postgraduate Dean	Signature	Date

ACKNOWLEDGEMENT

First and foremost, praise and thanks to the Almighty God for his mercies in allowing me to successfully complete this research.

I would like to express my sincere gratitude to my advisor, Dr. Rajkumer S, for his continuous support of my M.Sc. research, and for his patience, motivation, and enthusiasm. His guidance helped me in all the research and writing of this thesis.

I would like to express my thanks to Mr. Shanko Chura**,** who has supported me throughout my thesis work and sacrificed his valuable time to encourage me to work in my own way, and gave me the freedom to explore deeply this thesis. It would not have been possible to achieve the ultimate target of this thesis without his help. He gave me valuable assistance whenever I had a problem with my thesis.

Also, I would like to thank all the members of the School of Electrical and Computer Engineering (SoECE), especially the division of electronics and communication engineering, for providing such an excellent educational and research environment. I am thankful to all the students in the division of Communication Engineering who gave me all the knowledge.

A special thanks to Mir. Garoma Gebri, who supported me during my M.Sc. thesis when I was having emotional troubles.

Finally, I am thankful to my family, who has always let me go my own way and made me feel like I could do whatever I want, without any pressure.

TABLE OF CONTENTS

LIST OF TABLES

LIST OF FIGURES

LIST OF ABBREVIATIONS

3GPP	3rd Generation Partnership Project
4G	Fourth Generation
5G	Fifth Generation
ABG	Alpha Beta Gamma
AoA	Angle of Arrival
AoD	Angle of Departure
AR	Augmented Reality
BSs	Base Stations
CI	Close In
D2D	Device to Device
DL	Down Link
EHF	Extremely High Frequency
eMBB	enhanced Mobile Broad Band
FCC	Federal communication commission
FI	Floating Intercept
FSL	Free Space Loss
H_2O	Water
HetNets	Heterogeneous Networks
HPBW	Half Power Beam Width
IEEE	Institute of Electrical and Electronic Engineering
IMT	International Mobile Telecommunication
IOT	Internet of Thing

ITU	International Telecommunication Union
LOS	Line of Sight
MATLAB	Matrix Laboratory
METIS	Mobile and wireless communications Enablers for the Twenty-twenty Information Society
MiWEBA	Millimeter-Wave Evolution for Backhaul and Access
M-MIMO	Massive Multiple Input Multiple Output
MMSE	Minimum Mean Square Error
mMTCs	massive Machine Type Communications
mmWave	millimeter Wave
MPCs	Multi Path Components
NLOS	Non Line of Sight
O_2	Oxygen
PLE	Path Loss Exponent
QoS	Quality of Service
QuaDRiGa	Quasi Deterministic Radio Channel Generator
RF	Radio Frequency
RX	Receiver
SLs	Spatial Lobes
SSCM	Statistical Spatial Channel Model
SUI	Stanford University Interim
TCs	Time Clusters
TDD	Time Division Duplex

TX	Transmitter
UDNs	Ultra Dense Networks
UE	User Equipment
UHD	Ultra High Definition
UL	Up Link
ULA	Uniform Linear Array
UMi	Urban Micro
URLLCs	Ultra Reliable Low Latency Communications
V2V	Vehicular-to-Vehicular
VR	Virtual Reality
Wi-Fi	Wireless Fidelity
WLAN	Wireless Local Network
WPAN	Wireless Personal Area Network

ABSTRACT

Existing wireless communications in the sub-6 GHz bands are facing challenges from the growing demand for higher data rates and better quality of services. To satisfy these demands, the fifth generation (5G) mobile network would consider unused spectrum in the millimeter wave (mmWave) spectrum (30-300 GHz). The shortage of bandwidth in the sub-6 GHz band is solved using mmWave technology. Furthermore, mmWave provides significantly higher throughput, data rate, and capacity. Despite the fact that a huge bandwidth is employed, mmWave technology suffers from path loss, atmospheric attenuation, building penetration loss, diffuse scattering from rough materials, shadowing, and reflection loss. These leads to a decrease in the transmitted signal power. Therefore, an accurate and reliable channel model is important in the mmWave bands, particularly for the indoor environment. Moreover, by using technologies like beam-forming and others coupled with mmWave, the listed impairments are minimized. In this thesis, we analyze the performance of different path loss models (CI, free space, and two rays) at 38, 60, and 73 GHz carrier frequencies in terms of path loss with respect to the separation distance between transmitter and receiver. Additionally, we have evaluated the performance of the path loss with respect to the break point distance to enhance the received signal power and throughput. We have also done analysis of the directional power delay profile with received signal power, path loss and path loss exponent (PLE) at 38 GHz and 73 GHz mmWave bands for both LOS and NLOS by using uniform linear array (ULA) 2X2 and 64x16 antenna configurations using the channel model simulator (NYUSIM). The simulation results show the performance of different path loss models in the mmWave and sub 6 GHz bands. The path loss in the close-in (CI) model at mmWave bands is larger than that of free space and two ray path loss models, because it considers all shadowing and reflection effects between transmitter and receiver. Moreover, we have scaled up the received signal power and throughput of mmWave systems by using a large number of antennas at the transmitter.

***Key words**: 5G, mmWave, indoor environment, propagation characteristics, path loss, break point distance*

CHAPTER ONE

1 INTRODUCTION

1.1 Background

Wireless communications have progressed, and mobile data traffic is predicted to expand by 1000-fold over the next decade. The growing number of connected devices, the tremendous growth of mobile services and customer demands will put a tremendous strain on the existing wireless communication infrastructure. To address these concerns, the wireless industry is moving toward 5G cellular technology, which will boost capacity while also improving energy efficiency, cost, and spectrum use [1].

Mobile broadband has always been a key in the advancement of mobile communication systems, hence it is the main driving force behind 5G. Future 5G systems, on the other hand, are predicted to have a significantly larger societal influence than the previous system. As a result, they will focus on a wide range of use cases as specified in the 5G plan by ITU for 2020 and beyond. As indicated in figure 1.1, these use cases include eMBB, mMTCs, and URLLCs.

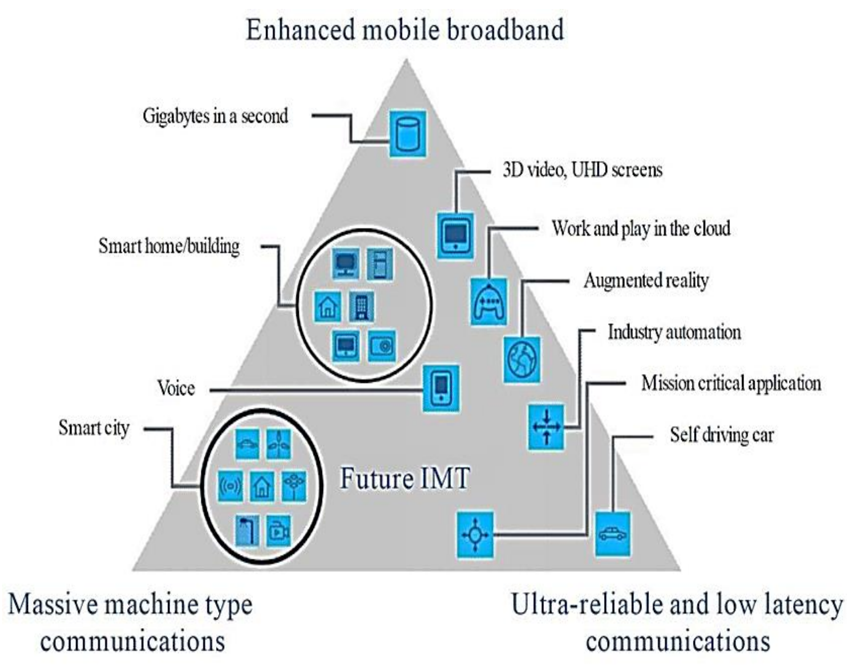

Figure 1.1: 5G Usage scenarios identified in IMT for 2020 and beyond [2]

The **eMBB** use case is characterized by broadband data access everywhere, from sparsely-populated areas to densely-populated areas, like indoor hotspots, stadiums, venues, and high-speed public transportation networks. The goal is to give the best possible user experience by enabling indoor and outdoor connectivity and providing high QoS internet even in difficult network situations. The other applications supported by this use case are AR, VR, and context recognition.

The **mMTC** use case's goal is to link everything to the internet. This massive connectivity will improve infrastructure automation and monitoring, allowing them to operate with little to no human interaction. As a result, mMTC use cases will enable IOT applications like smart homes and cities, as well as smart agriculture. In addition to these characteristics, mMTC should have a wide range of coverage and, most crucially, low power consumption and low-cost devices that are critical for achieving this use case goal.

The **URLLC** use case is designed for applications requiring very low latency, like remote healthcare, self-driving or autonomous vehicles, and factory automation. URLLCs are expected to have high reliability, continual availability, and high security because these applications frequently entail individual or public safety.

To achieve the 5G design targets, many technologies have been identified, including mmWave communications, M-MIMO, small cell deployment, full duplex relaying, and D2D communications. However, the information theory says three of the listed technologies highly achieve multiple orders of magnitude increases in system capacity: (i) UDNs: existing 4G wireless cellular networks have already embraced network densification, which is known as small cell technology, and a denser network can further enhance network capacity; (ii) Large amounts of bandwidth: moving to higher frequencies will offer a large quantity of bandwidth that can be used to increase capacity. mmWave communications, in particular, could be a promising candidate, with carrier frequencies ranging from 30 to 300 GHz; (iii) High spectrum efficiency: by deploying a large number of antennas at the BS (100 or more), M-MIMO can considerably enhance spectrum efficiency by utilizing available space resources [3].

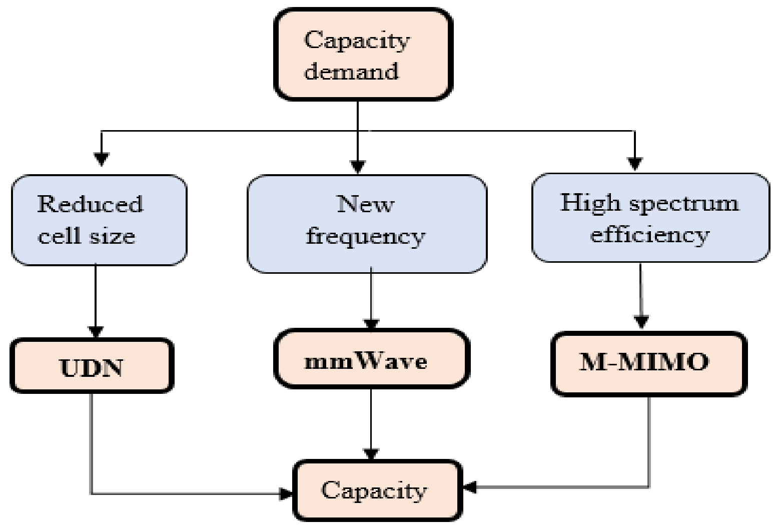

Figure 1.2: Three techniques to increase 5G system capacity

In many ways, these three techniques are related: Massive MIMO's high antenna gains assist in minimizing the path loss of mmWave signals. Smaller cell sizes are attractive for short-range mmWave communications, and the short wavelength of mmWave frequencies is appealing for M-MIMO since the physical size of the antenna array is minimized greatly [4].

In various recent studies on future mobile communications, mmWave communication has been recommended as the main technology for the development of the IOT in 5G and beyond, with more unused frequency bands and a high data rate [5]. The mmWave bands are the highest electromagnetic radiation radio frequency bands, with frequencies ranging from 30 GHz to 300 GHz with wavelengths ranging from 10 mm to 1 mm [6]. It is also known as EHF.

Millimeter wave carrier frequencies allow for larger transmission capacity distributions, which leads to a higher rate of information exchange. Because of the shorter wavelength (high frequency), mmWave utilizes unique spatial handling techniques and polarization, like: M-MlMO and adaptive beam-forming technologies are used [7].

There are various reasons why mmWave frequencies should be used in future 5G networks. The mmWave has a lot of spectrum, including the local multipoint distribution service at 28–30 GHz, 60 GHz, and the E-band, and 92–95 GHz, whereas the existing communication system (sub 6 GHz) operates in a congested and scarce band. The same frequency can be reused over short distances because of higher attenuation in free space and penetration in mmWave communications, which allows high throughput networks. At mmWave frequencies, antennas are so small in size that complicated antenna arrays and further integration onto chips or PCBs are possible. Due to the short range of transmission and narrow beam-width, the inherent security and privacy of mmWave communication is enhanced [8]. Therefore, we implement this technology for both the indoor and outdoor environment.

According to a recent study, 80 percent of wireless traffic will originate from indoor environments in the coming years. As a result, mmWave technology must be used to handle the massive data demand in the indoor environment. Generally, indoor communication originates in a LOS scenario, however, when the network becomes more congested, a NLOS scenario may occur. Therefore, the current 4G network is unable to handle the growing demand for data indoors due to its limited spectrum of microwave frequencies. Hence, 5G with mmWave could be a viable option for indoor networks [9]. But, when deploying mmWave in an indoor environment, understanding the propagation characteristics and channel impediments are important. The main impairments of mmWave propagation are path loss, reflection loss, and increased blocking effects because of weaker NLOS paths due to the availability of buildings, which are often made of concrete, bricks, glass, wood, and other home materials, as well as human. Moreover, the noise power is high because of the use of higher bandwidth [10].

Besides the listed impediments, attenuation is induced by absorption of air molecules, mainly O2 and H2O, which disturbs mmWave communication more significantly than microwave frequencies. But, for cells with a radius of less than 200 m, atmospheric absorption as well as rain attenuation do not result in extra path loss [9]. Despite suffering from the listed impairments, mmWave provides a huge bandwidth for short-range transmission, making it a preferable option for indoor wireless communication.

In this thesis, we considered different path loss models for the indoor environment at different carrier frequencies (38, 60, and 73 GHz). We chose these frequencies because most of the current research in mmWave focuses on the 28 GHz, 38 GHz, V band (60 GHz) and E band. We improved the received signal power and throughput by analyzing path loss in several path loss models with a distance between TX and RX and the path loss with break point distance for different heights of transmitter using MATLAB. We also compared the directional power delay profile with received signal power, path loss and path loss exponent (PLE) at 38 GHz and 73 GHz mmWave bands for both LOS and NLOS by using ULA 2X2 and 64x16 antenna configurations using the MATLAB based NYUSIM simulator.

1.2 Statement of the Problem

For nearly two decades, the 2.4 GHz and 5 GHz industrial Wi-Fi frequency bands have been utilized for short-range indoor wireless communications in offices, conference halls, hotels, and restaurants [11].

Due to the fact that people spend the majority of their time at home and at work, the majority of voice and multimedia services take place in an indoor environment. As a result, the capacity demand for indoor communications will continue to rise at an alarming rate, not handled by the current Wi-Fi radio band. In order to support the massive data flow, these situations require the use of more advanced indoor communication networks. The vast amount of unused frequency resources in the mmWave spectrum is being considered as one of the primary solutions to wireless network congestion. Hence, the frequency band in mmWave offers higher bandwidths for indoor wireless communication systems.

As a result, research has focused on the mmWave spectrum. However, because of its short wavelength, the mmWave travels and propagates through LOS communication, which means that physical objects like buildings, walls, humans, and home furniture can stop and affect these waves, in turn reducing the received signal power and throughput, especially in indoor communication. Recent studies have demonstrated that for small cell sizes on the order of 200 m and by implementing technologies such as Massive MIMO, Beam-forming, and directional antennas, the issues mentioned above can be minimized [12].

1.3 Objectives

1.3.1 General objective

The main objective of this thesis is to analyze the performance of mmWave communication using different path loss models to enhance the received signal power and throughput in an indoor environment.

1.3.2 Specific objectives

- To compare path loss at sub 6 GHz and mmWave frequencies.
- To evaluate the path loss of a two-ray model at different frequencies.

- Compare different path loss models at mmWave frequencies.
- To analyze path loss model with different first Fresnel zone break points.
- To analyze Fresnel zone break points with different mmWave frequencies.
- To compare the received signal power in LOS and NLOS scenarios at mmWave frequencies using different antenna configurations.

1.4 Significance

This work improves the received power of a communication system by minimizing the path loss effect. Hence, in this thesis we examined the path loss with different separation between TX-RX and breakpoint distances for different path loss models at different carrier frequencies, particularly for the indoor environment. There are many obstacles in this environment, such as home furniture, human beings, and ground reflection, that cause the transmitted signal to propagate in different directions, causing blockage and path loss, which reduces the received signal power and also throughput. As a result, path loss and blockage effects must be minimized. To minimize these problems, a large number of antennas are being considered.

1.5 Scope

This thesis focuses on enhancing the received signal power and throughput in an indoor communication system at different mmWave frequencies (38, 60, and 73 GHz) by analyzing the path loss at different separation distances and breakpoint distances. In mmWave there are many unused spectrums available. However, the path loss increases as the carrier frequency increases (short wavelength), because the signal propagates in different directions with the same or different time delays and angles due to obstructing objects between the transmitter and receiver whose sizes are larger than the size of the transmitted signal. As a result, the received signal power and throughput are reduced. Different path loss models have been proposed by different researchers. In this thesis, we used free space, two rays, and CI path loss models to analyze the effects of mmWave indoor communication at 38 GHz, 60 GHz, and 73 GHz carrier frequencies. Moreover, we compared the directional PDP at 38 and 73 GHz frequencies for both LOS and NLOS scenarios using ULA 2X2 and 64X16 antenna configurations.

1.6 Main contribution

The main contribution of this thesis is to evaluate the performance of mmWave communication from the perspective of two rays and multipath. Moreover, we have also derived path loss formulations as a function of break point distance.

1.7 Thesis organization

The rest of the thesis is organized as follows:

Chapter 2: Review of different literature on mmWave, M-MIMO/beam forming and small cell deployment and the existing works related to mmWave radio propagation in an indoor environment at different path loss models.

Chapter 3: System model and mathematical formulation for the indoor environment at different carrier frequencies by considering different path loss models.

Chapter 4: Simulation results and discussion of each of the results obtained.

Chapter 5: Conclusions and recommendations for future work.

CHAPTER TWO

2 LITERATURE REVIEW

2.1 Introduction to mmWave

The significant technological improvements in mobile and wireless communications systems have not kept pace with current spectrum availability for cellular networks throughout the years. The frequency ranges below 6 GHz are used by almost all mobile and wireless technologies. Hence, the frequency available in the sub–6 GHz band will be insufficient to supply the required capacity for future communication networks [13]. As a result, shift to the mmWave frequency bands, which offer wider bandwidths.

The mmWave spectrum is a band of the spectrum that spans from 30 GHz to 300 GHz and corresponds to wavelengths of 10 mm to 1 mm, which is between microwave and infrared. However, in the wireless sector, the frequency ranges beyond 6 GHz are referred to as the mmWave bands. Standard organizations, the FCC, and researchers are considering it as a means of bringing "5G" into the future by assigning larger bandwidth to enable faster, higher-quality video and multimedia content and services [14].

Since the first mmWave communications were demonstrated over a century ago, mmWave frequencies have been used in several applications, including radar remote sensing, satellite communications, and security systems to improve precision and resolution [15]. However, because of the harsh propagation constraints involved in mmWave communications, like shadowing, larger Doppler spreads, high penetration loss, and high air absorption, particularly for NLOS channels, mmWave technology is not used for terrestrial mobile applications [16].

Despite the propagation constraints, mmWave frequencies remain highly attractive for future cellular networks, especially for higher-output local area networks as well as personal area networks. Several recent studies have demonstrated multi-Gbps access communications using mmWave. The large bandwidth available at mmWave, coupled with various technologies, including beamforming, small cells, and M-MIMO, make the mmWave an attractive solution for dense networks and densely populated areas, particularly in an indoor environment [17].

2.1.1 Millimeter wave spectrum

When compared to the microwave, mmWave has a much larger frequency band (30-300 GHz). Despite the fact that some unfavorable bands, such as 57–64 GHz and 164–200 GHz, as shown in figure 2.1, are easily absorbed by O_2 and H_2O respectively, the appropriate bands for mmWave communications are still above 150 GHz, and more than 150 Gb/s can be attained across the entire range.

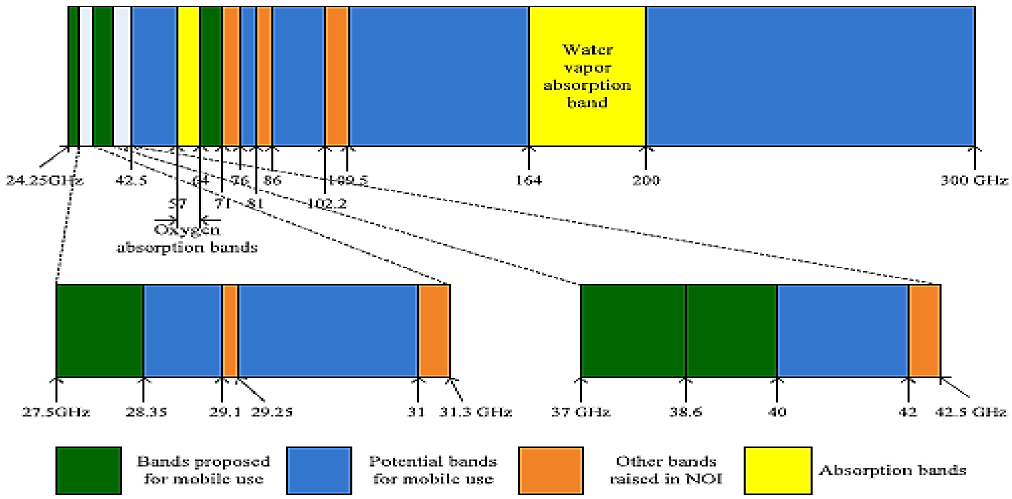

Figure 2.1: Millimeter wave spectrum, along with O_2 and H_2O absorption band [18]

The mmWave spectrum is divided and named into several bands with related frequency ranges and wave lengths, as shown in table 2.1. Some applications have been considered for some of these bands. Satellite communications, astronomy, and terrestrial microwave communications all use the Q band, which ranges from 30 GHz to 50 GHz. 60 GHz is a portion of the V band that runs from 50 to 75 GHz. It is used for unlicensed wireless communications and is best for high-speed indoor communications and short-range high-resolution radar sensors due to its high O_2 absorption. In fronthaul and backhaul networks, portions of the E band, including 71 GHz to 76 GHz, 81 GHz to 86 GHz, and 92 GHz to 96 GHz, are used. Satellite communications and deep space research can both benefit from the W band, which has a short wavelength.

Table 2.1: Frequency band and range in microwave, mmWave and Infrared [19]

Wave name	**Frequency bands**	**Frequency range (GHz)**	**Wavelength (mm)**
Microwave (1-30 GHz)	**L**	1-2	300-150
	S	2-4	150-75.00
	C	4-8	75.00-37.5
	X	8-12	37.5-25.00
	Ku	12-18	25.00-16.67
	K	18-26	16.67-11.54
	Ka	26-40	11.54-7.50
Millimeter-wave (30–300 GHz)			
	Q	30-50	10.00-6.00
	U	40-60	7.50-5.00
	V	50-75	6.00-4.00
	E	60-90	5.00-3.33
	W	75-110	4.00-2.73
	F	90-140	3.33-2.14
	D	110-170	2.73-1.76
	G	110-300	2.73-1.00
Infrared (IR)	300 GHz – 470 THz		

Millimeter wave bands are classified in to three categories [20]:

- **Licensed band**

These bands are used for mobile and fixed wireless access. Individual companies pay a license fee for the right to transmit at a specific frequency within a specific geographical area for these bands. In exchange, the users can be guaranteed that their transmission will be uninterrupted. The cost of getting a connection license is high. It may take a long time to get a license from the government, unlike lightly licensed bands.

- .**Lightly Licensed band**

These bands require a license from the FCC, which can be obtained through performing frequency coordination, issuing of a public notice, and submission of an application. This procedure ensures nobody else is utilizing the same or a frequency that will interfere with current systems. The cost of obtaining a connection license is low, and it may be done in a couple of weeks. Microwave link operators with a light license are granted exclusive usage of a portion of the band in a specific direction across a defined geographic area. When licensed radios experience interference, the problem is usually rectified with the help of the regulating agency. The millimeter bands 11, 13, 18, 23 GHz, and (70/80 GHz) are lightly licensed bands and are mainly used for point-to-point backhaul.

- **Unlicensed band**

Unlike lightly licensed and licensed bands, it does not require a government license. It is available without charge**.** The 60 GHz (V band) is a license-free frequency that can be utilized for point-to-point and point-to-multipoint backhaul as well as wireless access. The frequency distribution of the V band varies by country. In the United States, it consists of 14 GHz (57-71 GHz). This is 15 times more than the total amount of unlicensed Wi-Fi spectrum in the lower bands. Whereas, in Europe, it is 9 GHz (57-66 GHz).

2.1.2 Opportunities in mmWave

Besides the larger amount of bandwidth, mmWave has a number of advantages over conventional radio waves. These are:

- **Larger Antenna Array**

Because of the short wavelengths of mmWave communications, a large number of antennas can be utilized in a small space. This has important implications for antenna systems, as low-cost fabrication technology and compact integration allow for cost savings and production scale. At the same time, the beam-width narrows when there are multiple antenna elements. The benefits of this characteristics include increased security and greater resistance to co-user interference [18].

- **Channel Reciprocity**

Because the frequency bands for mmWave communication are unpaired, it uses a TDD scheme, which means that DL and UL communications use the same frequency but at different times. The UL and DL propagation channel characteristics are closely associated in these systems when the

DL and UL communications are conducted at a specified period of time, called the channel coherence time. This process is known as channel reciprocity [20].

- **Densification**

When mmWave coverage is desired in a particular area, a higher density of mmWave cells is expected than sub-6 GHz cells are employed to achieve the desired coverage. The mmWave band can give faster data speeds and capacity while still providing enough coverage due to its higher cell density [20].

2.2 Propagation characteristics of mmWave

The propagation characteristics of mmWave frequencies are different from the conventional sub-6 GHz bands. Moreover, the radio wave propagation characteristics differ from one frequency band to another. As a result, in order to design future mmWave communication systems, the channel characteristics of indoor, outdoor, cellular, front-haul, and backhaul systems must be properly analyzed [21]. The major propagation characteristics of mm waves are illustrated in figure 2.2.

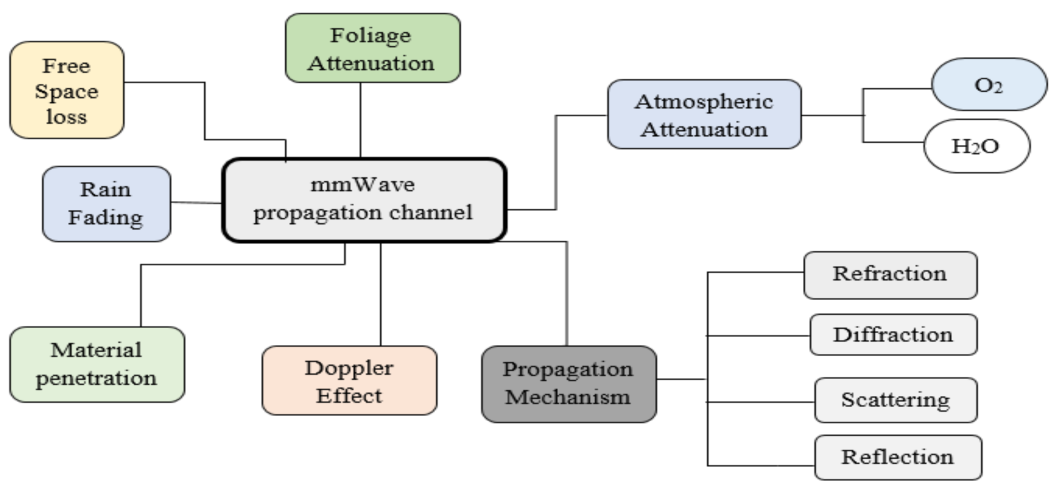

Figure 2.2: Millimeter wave propagation characteristics [22]

- **Free space loss**

The FSL is the loss of the transmitted signal strength as it travel in free space. The free space loss between two communicating isotropic antennas is given by:

$$FSL[dB] = 92.4 + 20\log_{10} f[GHz] + 20\log_{10} d[Km] \tag{2.1}$$

Where d is separation distance between transmitter and receiver in kilometers (km) and f is operating frequency in GHz.

The FSL has a linear relationship to both the separation distance and the carrier frequency, according to the given equation. When a carrier frequency moves into the mmWave frequency bands, the FSL increases rapidly in comparison to the sub-6 GHz band.

- **Atmospheric attenuation**

When molecules absorb a portion of the power carried by propagating waves and vibrate according to the carrier frequency, atmospheric attenuation, also known as gaseous attenuation, occurs. O_2 and H_2O are the two main absorbing gases at mmWave frequencies. The densities of gaseous absorption depend on several factors, including temperature, pressure, altitude, and, most significantly, the operational carrier frequency.

Figure 2.3 shows a simplified and combined result of O_2 and H_2O absorption in the mmWave frequency band. The O_2 absorption maxima are observed at 60 GHz with a loss of 15 dB/km and at 119 GHz with a loss of 1.4 dB/km. The O2 absorption loss can be further minimized by operating at short distances. The O2 absorption at 60 GHz and 119 GHz is reduced to 1.5 dB and 0.14 dB, respectively, when the cell range is reduced from 1 km to 100 m. Moreover, figure 2.3 shows that H_2O molecules may resonate at frequencies of 23 GHz, 183 GHz, and 323 GHz, with losses of 0.18 dB/km, 28.35 dB/km, and 38.6 dB/km, respectively. As a result, for future mmWave indoor communication systems, atmospheric losses should not be a major concern [23].

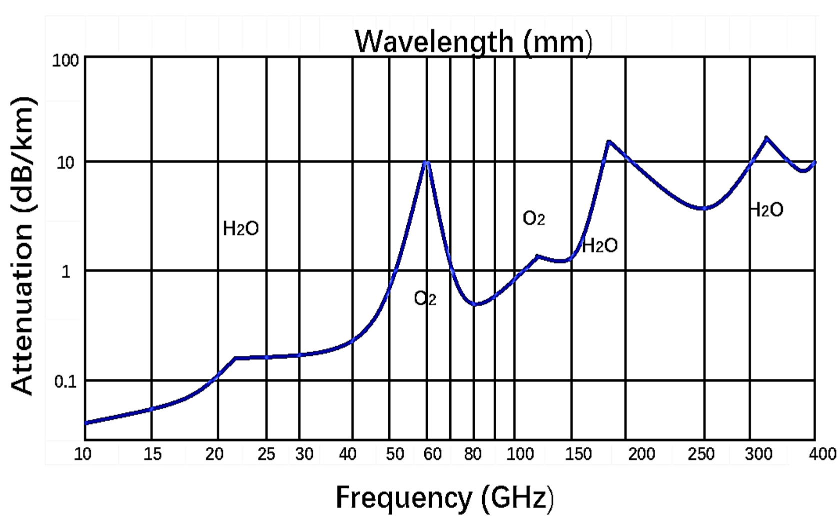

Figure 2.3: Oxygen and water absorption at mmWave frequency [12]

- **Rain attenuation**

The precipitation attenuation and losses due to rain are considerable for mmWave. At mmWave frequencies, raindrops and the size of the transmitted signal wavelengths are nearly the same. As a result, raindrops easily block mmWave communications, causing the signal's energy to be scattered and its strength to be lost [24].

The rain attenuation in mmWave and targeted sub-100 GHz bands for 5G is more problematic than rain attenuation in conventional microwave networks, with a maximum attenuation of nearly 30 dB/km for very heavy rainfall (100 mm/h). Moreover, it has different effects depending on the mmWave frequency ranges. The path loss due to rain attenuation is not considerable for a short range of communication on the order of 200 m. Therefore, higher mmWave frequencies are used in indoor environments and dense urban environments with cell sizes of less than 200 m [25].

- **Foliage loss**

Foliage attenuation is an important attenuating factor in mmWave communications. The existence of vegetation between the TX and RX induces extra signal loss, which can negatively affect the QoS of a wireless communication system. The depth of the vegetation component determines the intensity of foliage attenuation. A single tree has a smaller influence than numerous trees. Furthermore, radio signals are attenuated more severely by a forest than by several trees [26].

- **Material penetration**

The mmWave frequencies are susceptible to penetration loss, and in comparison to sub-6 GHz, they can't penetrate most solid materials well, including walls, doors, and room furniture. As a result, mmWave communications are easily blocked, particularly in densely urban areas with many buildings and a large number of people [22]. The mmWave signal's frequency, antenna polarization, angle of incidence, surface roughness, permittivity of material, and thickness of material all have an impact on penetration loss [27].

When mmWave signals travel from indoors to outdoors, the penetration loss is roughly 74 dB because of the inability of these signals to penetrate building materials. Similarly, high penetration loss has occurred when mmWave signals travel from outdoors to indoors. Therefore, these propagations may experience a large penetration loss, reducing the data throughput, spectrum efficiency, and energy efficiency. As a result, the majority of BSs will not be able to provide indoor mmWave coverage. Hence, to achieve indoor-to-outdoor coverage and vice versa, heterogeneous networks, repeaters, and relays are required [27].

- **Doppler spread**

The Doppler shift occurs when the frequency of a wave changes as the receiver moves away from and towards the BS. When the transmitter and receiver are moving towards each other, the Doppler shift is positive (higher frequency), but when they are moving apart from each other, it can be negative (lower frequency). The Doppler shift is given by [28]:

$$D_f = \frac{f_o * v}{c} * \cos\theta \tag{2.2}$$

Where v is relative velocity of the transmitter and receiver, f_o is the carrier frequency, c is speed of light in air (3*10^8 m/s), and θ is an angle that related to the direction of travel.

The Doppler spread is the range shifting up to the maximum and down to the minimum. Which is obtained from maximum Doppler shift. The maximum Doppler shift is:

$$D_{f\max} = \pm f_c \frac{v}{c} \tag{2.3}$$

Then Doppler spread becomes:

$$B_d = 2 * D_{f\max} = \frac{1}{T_c} \tag{2.4}$$

Where T_c coherent time of a channel and $D_{f\max}$ maximum Doppler shift.

According to the equation, the coherent time of a channel and frequency have an inverse relationship for a given user mobility, hence it is very small in the mmWave band, resulting in rapid channel fluctuations and inconsistent connectivity. According to some studies, at 60 km/h and 60 GHz, the Doppler spread is above 3 kHz, implying that the channel will shift on the order of hundreds of microseconds, much faster than current cellular systems [29].

- **Human blockage**

Because humans operate as the greatest barriers, reflectors, and scatters, their presence has a serious effect on the propagation characteristics of mmWave signals. The reason behind this problem is that the size of the human body is quite large in comparison to the mmWave signal.

Furthermore, when mmWave comes into contact with the human body, it experiences low penetration loss, whereas reflection and scattering, result in high losses.

- **Propagation mechanism**

The major causes of NLOS propagation between TX and RX are refraction, diffraction, and scattering. In this scenario, the transmitted signals still reach the receiver due to reflections from nearby objects, bending, or diffraction. Reflection and scattering occur when the barriers between TX and RX are larger than the propagating signal's wave length. As a result, short-wavelength mmWave signals are subjected to more shadowing and reflection and less diffraction [30].

The short wavelength of mmWave signals causes the reflecting surface to appear rougher, resulting in more signal diffusion and less specular or direct reflection, as seen in figure 2.3. As a result, diffuse reflection results in lower received transmission power than specular reflection.

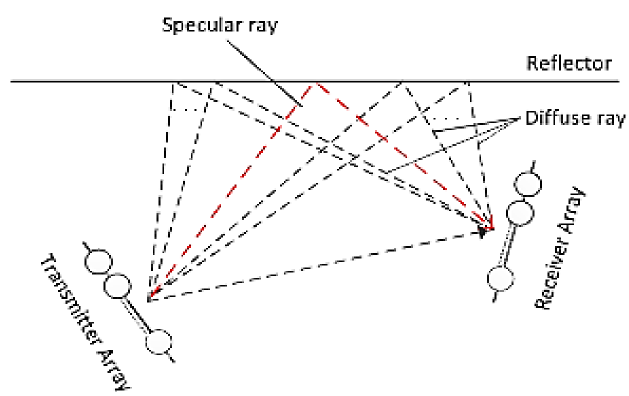

Figure 2.3: Propagation mechanism, namely specular reflection and diffuse scattering [30]

2.3 Channel modeling in Millimeter wave

Before constructing a channel model for any frequency range, it's necessary to understand radio propagation characteristics. Accurate channel modeling is required for creating an effective communications system operating in the mmWave bands, as well as developing innovative approaches that can fit to the propagation characteristics of these frequency bands [22].

Depending on the modeling approach, [22] presents a possible classification of channel models. As shown in figure 2.4, this classification divides channel models into two major groups: physical and analytical models. Analytical models represent the communication between a TX and RX mathematically and are usually utilized for algorithm development and system analysis, whereas physical models use electromagnetic characteristics to represent communication and can realistically reproduce channel characteristics depending on the complexity.

Physical channel models are further classified into two, as shown in figure 2.4, stochastic and deterministic models. Deterministic models are well-known for their accuracy in forecasting channel properties in a deterministic manner, but they come at a high cost in terms of computation and modeling complexity. These models are utilized when the propagation environment is known and they are particularly specific to that environment. Ray-tracing, in which each multipath component is represented as a ray, is the most extensively used technique in deterministic models. Ray tracing is often done with a standalone software program to simulate a desired channel situation with all known environmental conditions and kept in the system. Another benefit of deterministic models, particularly ray tracing models, is that they may be quickly used to predict the features of a new environment if no measurements for that situation are available. This saves a lot of money on measuring campaigns.

The Stochastic channel models, on the other hand, generate the channel's impulse response, which describes the spatio-temporal properties of the channel's MPCs based on the measurements taken in various situations and conditions. Large-scale and small-scale fading characteristics are commonly described using PDFs of channel parameters. These channel models are simple models which take a short time and have reduced complexity in computational, making them suitable for systems design and simulation.

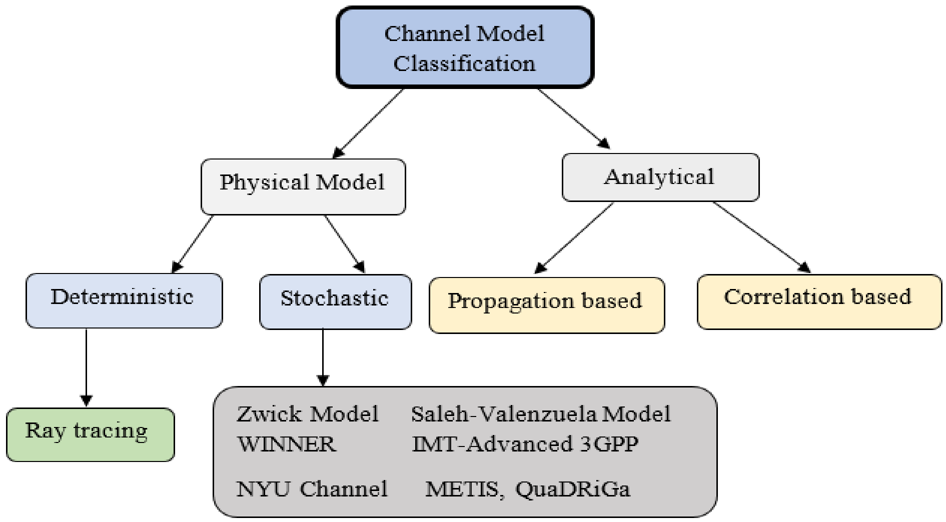

Figure 2.4: Channel model classification [22]

2.3.1 Current channel model in Millimeter Wave

METIS: developed the mmWave channel model based on measurements taken in various situations at various frequencies that are not sufficiently represented by existing channel models. The METIS project suggested three channel models, such as stochastic, map-based, and hybrid (which is a combination of the two models) to meet the needs for flexibility and scalability. The stochastic model is appropriate for frequencies up to 70 GHz, whereas the map-based model is appropriate for frequencies up to 100 GHz. In these models, ray-tracing techniques and measurement-based results are used to generate large-scale and small-scale fading characteristics, respectively. The project includes different propagation environments, including indoor office, urban micro-cell, urban macro-cell, D2D, V2V, and rural macro-cell [31].

MiWEBA: developed to characterize the 60-GHz outdoor multipath channels, is characterized by the superposition of a few strong deterministic pathways and numerous very weak random rays, which use a quasi-deterministic channel model. MiWEBA is capable of supporting mmWave massive MIMO communications and beamforming. This channel model is applicable only to the specific situation under consideration and can't be applied to other situations because the quasi-deterministic modeling technique requires a precise description of the situation [32].

QuaDRiGa: is a 3D geometry-based stochastic channel model which was created primarily for modeling MIMO channels in specific network configurations. QuaDRiGa supports the mmWave spectrum from 0.45 GHz to 100 GHz, with a bandwidth of up to 1 GHz, and provides spatial consistency primarily through the correlation of large-scale and small-scale characteristics. This channel model incorporates the characteristics of the 3GPP spatial channel model extension and WINNER channel models, and also new modeling techniques, to provide quasi-deterministic receiver-movement-multi-link tracking in changing situations [33].

The 3GPP Model: is a recently suggested 3D representation of the 3GPP channel model, specifically the 3GPP TR 38.900 3D model, which is an expansion of the 3GPP TR 36.873 channel, which is typically utilized for sub-6 GHz. The current model supports frequency bands up to 100 GHz in a variety of scenarios, including urban macro cells, urban micro cells, D2D, indoors, and so on. In addition to the azimuth angle dimension, this 3D model can also capture the channel's elevation angle dimension.

NYUSIM: a MATLAB-based-open source channel model simulator created by NYU WIRELESS. NYU WIRELESS is an academic research institute focusing on mmWave technology. It can operate at up to 100 GHz carrier frequency and 800 MHz RF bandwidth. This simulator employs a SSCM for broadband mmWave wireless communication, which generates channel responses and accompanying AoA/AoD power spectra using TCs and SLs. Because of the high gain directional antennas of MIMO, NYUSIM captures multipath components in a TC method from diverse pointing angles. These characteristics are not taken into account in the WINNER and 3GPP models. Furthermore, under the 3GPP/WINNER model, the number of measured path loss samples and their respective distances have a significant impact. NYUSIM, on the other hand, employs both a close-in distance (CI) parameter and a PLE. As a result, better stability is achieved in a variety of environmental conditions. Therefore, in comparison to the 3GPP and also other channel models for mmWave bands, it is more realistic [34].

2.4 Beamforming technology

Beamforming enhances the BS antenna gain and helps focus the energy of antennas in a particular direction while avoiding interference from other sources. When transmit and receive antennas are used to achieve beamforming gain, the path loss of mmWave transmission can be comparable to that of a conventional carrier frequency band. The short wavelength, in particular, enables the construction of arrays of antennas with several other elements in a compact space that can focus energy in narrow beams in adjustable directions. There are three beamforming techniques: digital, analog, and hybrid. Each of these techniques has a major impact on energy consumption, attainable beamforming gain, complexity, and runtime [12].

2.4.1 Analog beamforming

Analog beamforming is an effective method of creating high beamforming gain with a large number of antennas allowed in mmWave bands. All of the antennas share the same radio frequency chain, and the beam alignment phase is simplified. As shown in figure 2.5, by sending pilots in a specified set of directions (codebook) and modifying the phase shifters for each antenna element, the transmitter and receiver search for the optimal TX-RX beam combination that optimizes the gain [35]. Analog beamforming employs complex coefficients to control the RF signals using phase shifters or variable gain amplifiers, with the goal of compensating for the mmWave bands' significant path loss. It supports single-stream transmission.

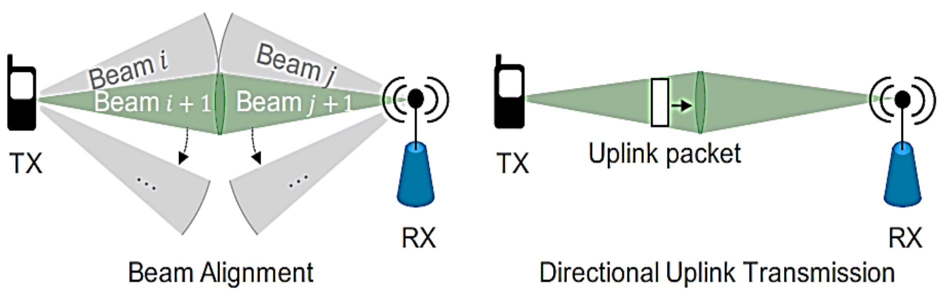

Figure 2.5: Beam scanning for the alignment phase with a predefined set of beams followed by directional uplink transmissions [35]

2.4.2 Digital beamforming

Digital beam-forming uses digital precoding to multiply a certain coefficient to the modulated baseband signal per RF chain to boost capacity utilizing various MIMO approaches. Each antenna has its own radio frequency chain. In general, digital beamforming is more flexible, has a higher beam-forming gain, supports multi-stream transmission, and has higher performance. However, because each output has its own RF chain, it will be more complicated and expensive.

2.4.3 Hybrid beamforming

Hybrid beam-forming offers a good compromise between all digital and all analog beamforming structures [36]. When a large number of antennas are required, as in the mmWave, hybrid beamforming is preferable, because it is a trade-off between flexibility/cost, simplicity, and performance.

A hybrid beamforming architecture is shown in figure 2.6 at both the TX and RX. In this design, the narrow beams created using analog beamforming (phase shifters) mitigate the significant path loss at mmWave bands, while digital beamforming gives the flexibility needed to conduct advanced multi-antenna approaches like multi-beam MIMO.

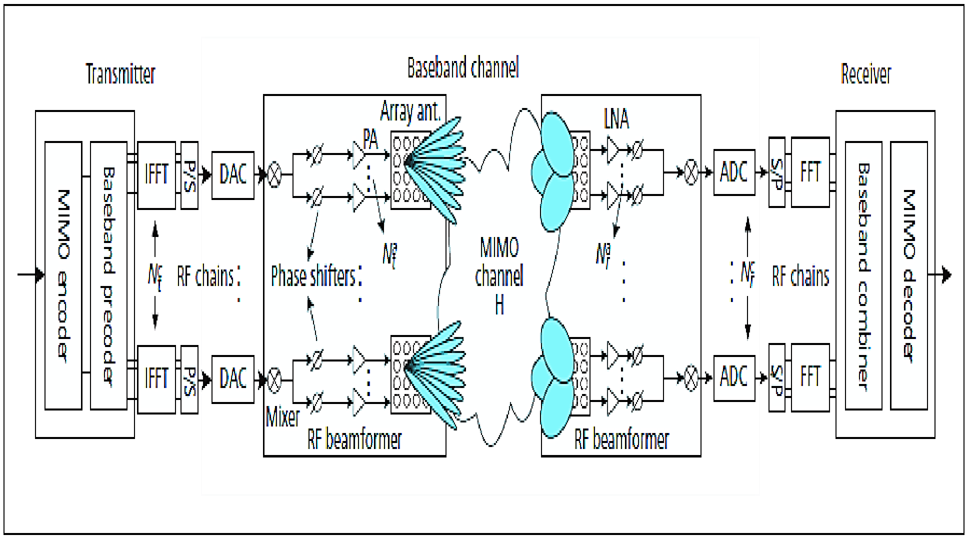

Figure 2.6: Hybrid beamforming architecture [36]

2.5 Small cell deployment

The mmWave networks can be made very dense to overcome blockages, and can benefit from the current trend of moving cellular systems to a large number of small–cells, which we call network densification. The concept of network densification employing small–cells, as shown in figure 2.7, is easier to construct and more cost-effective because it uses less transmission power and serves a small number of users. A network including these different cell sizes is called a HetNets. HetNets, which allow home users to buy small cell BSs and place them in areas with poor reception [37].

Furthermore, because small–cells are placed much closer to the UEs than typical macro–cells, higher coverage is attained. Small–cell deployment, varying from micro–cells to femto–cells, will boost the spectrum reuse ratio as cell sizes decrease. As a result, HetNets are predicted to enable considerable significant improvements in spectral efficiency [38]. HetNets may incorporate other components such as remote radio heads (RRHs), relays, and multi–hop relays in addition to these small–cells, all of which will help to improve network performance.

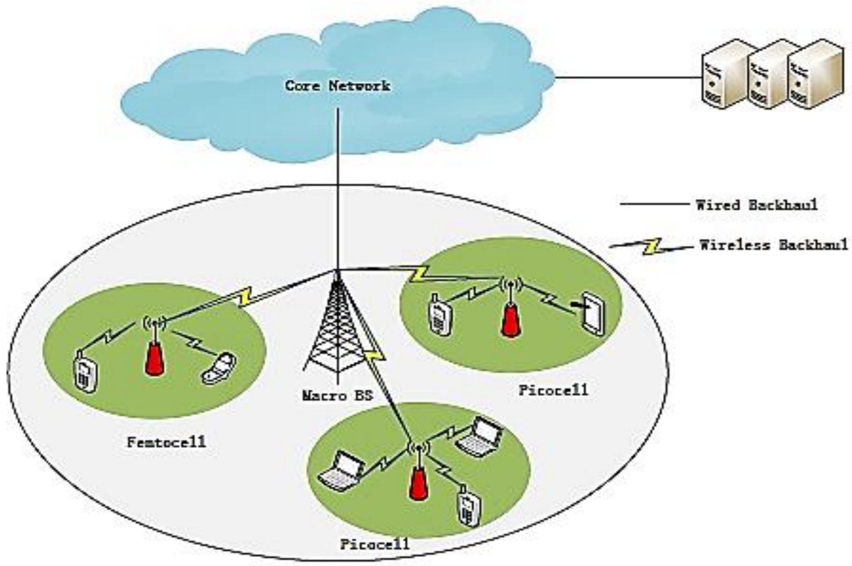

Figure 2.7: Small cell densification

5G mmWave Small cells are employed in the following two target situation:

- **Capacity Enhancement**

Small cells are placed inside the coverage of an overlay macro-cell in this scenario to boost the overall network's data throughput. As seen in figure 2.8.a, the small cell's coverage overlaps that of the macro-cell. This configuration aims to increase the network's overall capacity while also increasing the capacity of a hotspot within an anchor macrocell's coverage.

- **Coverage Extension**

To expand the coverage of the 5G network, small cells are put at the edge of macro-cells. The small cell's coverage can partially overlap with the coverage of the covering macro-cell in this situation, as seen in figure 2.8.b, expanding the 5G network's coverage. This arrangement is primarily intended to improve the user's perception of service availability. This design is suitable for deployment in both indoor and outdoor environments where better QoS and data throughput are required at the cell edge.

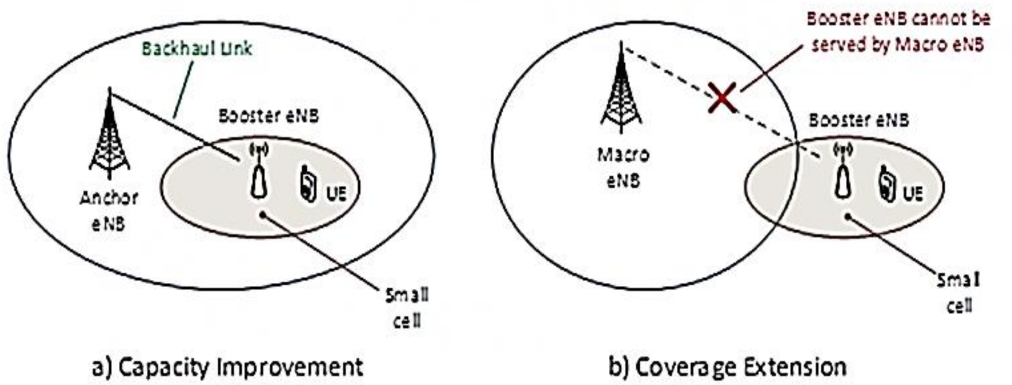

Figure 2.8: mmWave small cell underlying for capacity and coverage enhancements [20]

2.6 Applications of mm Wave communications

- **Small cell access**

Small cells placed as WLANs or WPANs beneath macro cells are a possible approach to increasing capacity in 5G cellular networks. mmWave small cells can enable multi-gigabit rates and wideband multimedia applications due to their large bandwidth [12].

- **D2D communications**

The use of directional antennas in mmWave communication introduces a new characteristic to the system: narrow directed beams that minimize fading, multipath, and interference. The mmWave devices can operate more effectively in noise-limited rather than interference-limited situations because adaptive arrays with narrow beams reduce interference. This mmWave feature is used in device-to-device communications that allows a user equipment to interact directly with another user equipment in close proximity over a D2D link without having to go through the central BS. The mmWave 5G cellular network design with device-to-device communications is shown in figure 2.9. These communications in close proximity reduce power and enhance spectrum efficiency, hence they should be activated in millimeter wave cellular networks to allow context-aware applications that need to discover and converse with adjacent devices.

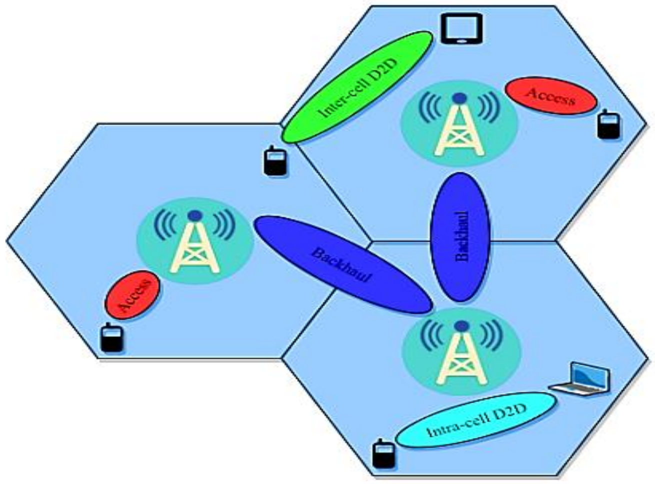

Figure 2.9: mmWave cellular network architecture with D2D communications enabled [39]

- **Wireless backhaul**

Fiber-based backhaul is expensive to connect 5G BSs to each other and to the network because small cells are widely distributed in the next generation of cellular networks. Due to the high bandwidth available, wireless backhaul in mmWave bands such as the 60 GHz and E-band can provide multiple gigabit per second data speeds and can be a feasible backhaul solution for small cells. The E-band backhaul, as indicated in figure 2.10, allows high-speed communication between small cell BSs or between BSs and the gateway.

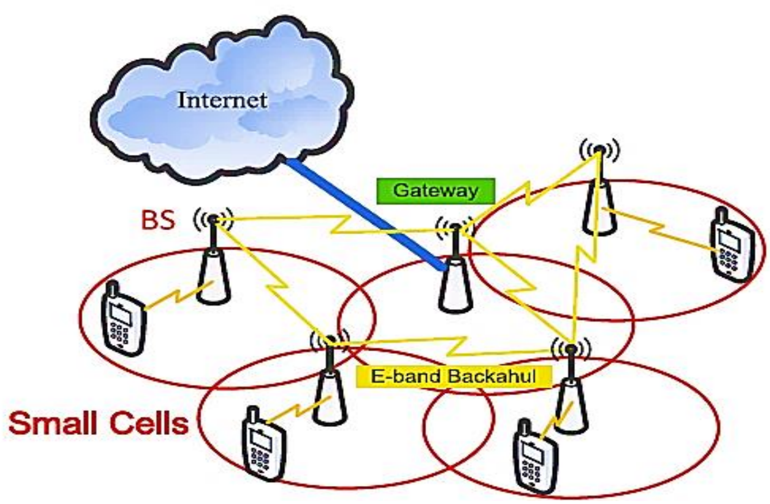

Figure 2.10: E-band backhaul for small cells densely deployed [12]

2.7 Related works

In [40] for both LOS and NLOS scenarios, the characteristics of mmWave multipath propagation based on path loss, delay spread, and received power for several mmWave bands at 28, 39, 60, and 73 GHz for indoor communication have been analyzed. They consider the effects of different building materials, frequency sensitivity materials, and multi-floor indoor communication systems on signal propagation characteristics. The researchers employed wireless insite software to assess the performance of each frequency; the results show an inverse relationship between separation distance, frequency, and both delay spread and received power. Furthermore, path loss increases as the separation distance and frequency increase for a variety of reasons related to antenna directionality and characteristics.

In [41], the channel propagation characteristics of a 5G system in LOS and NLOS scenarios are presented. Based on the data they collected in an indoor environment at 3.5 GHz and 28 GHz, the diffraction loss (DL) and frequency drop (FD) are evaluated. The parameters for path loss are determined using several path loss models (CI and ABG) for single and multi-frequencies. The power delay profile, excess delay, and root mean square (RMS) delay dispersion of received paths are analyzed. At both frequencies, the PLE in the indoor environment is less than the free space path loss exponent for the LOS scenario, according to the results of the path loss models. However, in the NLOS case, where the PLE value is higher than the free space PLE, the received power is reduced.

In [42], an analytical approach for evaluating the levels of propagation losses experienced by mm-Wave signals in an indoor environment is presented. The analysis used the free space model, the ABG Path loss model, the CI model, the SUI Model, and the Ericsson Model. To evaluate the varying signal path loss, different mmWave frequencies, 28, 38, 60, and 73 GHz, were deployed with distances ranging from 1 m to 5 m. To determine the varying penetration losses, different physical propagation mediums were evaluated. The results showed that the ABG propagation model, which has the lowest penetration loss, is the most suitable for indoor applications, followed by the CI model. The Ericsson model was characterized as having the highest penetration loss.

The statistical channel modeling for LOS and NLOS scenarios in an indoor environment using the NYUSIM simulator is presented in [9]. Comparing both directional and omnidirectional PDP with respect to path loss, received signal power, and PLE for both scenarios using a ULA 4x4 antenna configuration at 60 GHz. The results showed that the received signal power in directional PDP is better than in omnidirectional PDP for both scenarios.

In [43], a comparison of CI and FI models with single- and multi-frequency path loss models at 28 and 73 GHz in three indoor office designs, including corridor, open-plan, and closed-plan, was made. The results show that employing single and multi-frequency path loss models with close-in free space reference distances simplifies path loss calculation and prediction across a wide range of distances and frequencies. Whereas, the high variances in the FI and ABG model parameters leads to large inaccuracies.

The mmWave propagation characteristics at 26, 32, and 39 GHz frequency bands in the corridor indoor scenario with LOS conditions using two antenna configurations are presented in [44]. A horn antenna was utilized in transmission, while horn and omnidirectional antennas were employed in reception. The path loss in the horn configuration is higher than in the Omni. On average, path loss is larger at higher frequencies, as expected. In all cases, the path loss exponents are less than 2, confirming a waveguide-like propagation effect in LOS conditions.

In [45] at 28 and 73 GHz, mmWave propagation with respect to path loss was examined in an office environment, for transmit powers of 24 dBm and 12.3 dBm, respectively. PDPs were obtained for 48 TX-RX position pairs with a distance range from 3.9 to 45.9 m. For both co-and cross-polarized antenna designs, directional and omnidirectional path loss models, as well as RMS delay spread, are given for LOS and NLOS conditions. In both LOS and NLOs scenarios, omnidirectional PLEs are larger than directional PLEs for vertically polarized antennas. They also used a technique known as beamfoarming at the BS and UE to enhance received signals and expand coverage by searching for the strongest transmitter-receiver angle directing link at each receiver position.

The large-scale path loss model for the indoor environment is presented in [46], for 4.5, 28, and 38 GHz bands. The effect of path loss on 5G signals transmitted over these frequency ranges was analyzed. The CI model is more efficient than the FI model for single-frequency path loss. As a result, the FI model does not accurately describe the channel in a LOS and NLOS scenario. Moreover, the multi-frequency ABG path loss model showed that all frequency slope values (γ) in LOS and NLOS indicate an undesirable level of attenuation as frequency increases.

From the reviewed related works, researches were done on different indoor environments using different path loss models like CI, FI, ABG, and SUI using different antenna configurations for LOS and NLOS. Unlike these works, this thesis focuses on evaluating the performance of mmWave communication from the perspective of two rays and multipath. Also, analyzing the path loss at different separation distances and breakpoint distances for CI, free space and two rays for different mmWave bands. Additionally, by adding a large number of antennas at the TX and RX with a co-polarized antenna configuration, the received power of the directional PDP for both LOS and NLOS scenarios is compared.

CHAPTER THREE

3 SYSTEM MODEL

In this thesis, different related literature is reviewed from different journals, IEEE papers, and books on 5G technologies focusing on mmWave, beam-forming techniques, and propagation characteristics of mmWave, particularly in an indoor environment. Depending on this literature and having the statement of the problem, to achieve the desired objectives, the following methodologies are designed:

1) System models and different mathematical formulations
    - A Mathematical model for calculating path loss for different path loss models.
    - A mathematical model for calculating the breakpoint distance from the first Fresnel zone.
    - Derive mathematical expressions that relate the path loss to the break point distance.
2) Identify input parameters for the simulation
3) Perform simulation using MATLAB R2015b and NYUSIM simulators
    - Simulation for path loss analysis of different frequency bands (38, 60, and 73 GHz) for the indoor environment using different path loss models (free space, CI, and two rays).
    - Simulation for path loss analysis of different frequency bands with varying breakpoint distance.
    - Simulation for break point distance at different carrier frequencies, transmitter and receiver height.
    - Simulation for directional PDP at 38 and 73 GHz using 2x2 and 64x16 antenna configurations for both LOS and NLOS scenarios.

3.1 System model and Mathematical Formulation

In figure 3.1, a system model for an indoor environment is displayed, with both LOS and NLOS conditions. In an indoor environment, the microcell's base station provides mmWave access link connectivity to all UEs and access points. When the environment is clear of obstructions and the UE is within LOS of the BSs, the communication system continues with higher signal quality. However, any obstacle, such as a human blockage, ground reflection, and others, causes communication to be interrupted or lost. Furthermore, these obstacles lead to increased path loss, which leads to decreasing received power.

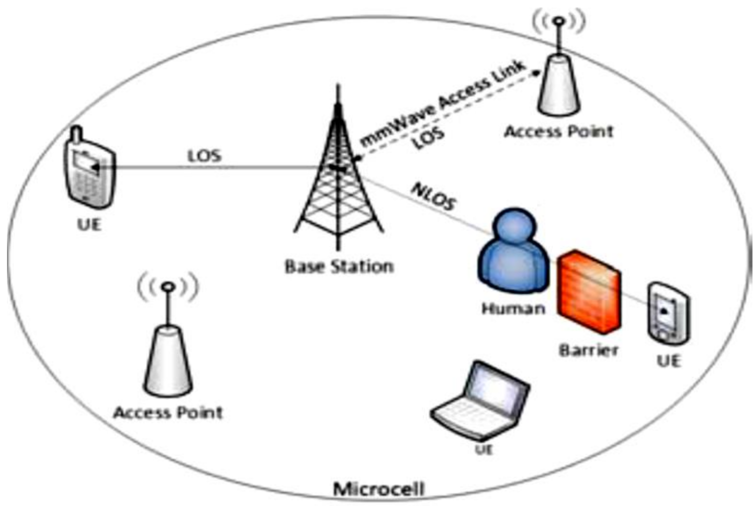

Figure 3.1: An indoor mmWave network scenario for 5G systems [9]

- **Path loss model**

To effectively analyze the performance of 5G systems, particularly in an indoor environment, different path loss models will need to be built across a wide range of frequency bands and operating scenarios. There are various path loss models, which are explained in the following sections.

3.1.1 Free space path loss model

In the free space path loss model, there are no obstruction objects between the TX and RX antennas and a clear LOS path exists between them [47]. From Friis's free space equation, the received power is given as:

$$P_r(d) = P_t G_t A_r \frac{1}{4\pi d^2} \tag{3.1}$$

Where P_r is receiver Power, P_t is transmitter Power, G_t transmitter Antenna Gain, A_r is effective area of a receiver Antenna and d is distance between transmitter and receiver. According to the given equation, the received power is inversely proportional to the separation distance between the user and the base station. The Effective area has a relationship with the receiver antenna gain Gr, which can be written as:

$$G_r = \frac{4\pi}{\lambda^2} A_r \tag{3.2}$$

Now from equations (3.1) and (3.2), it can be deduced that:

$$P_r(d) = P_t G_t G_r \frac{\lambda^2}{(4\pi d)^2}$$
$$P_r[dBm] = P_t[dBm] + G_t[dB] + G_r[dB] - PL(d)[dB] \tag{3.3}$$

Where P_r is received single power, P_t is transmitted signal power, G_t is transmitter antenna gain, G_r receiver antenna gain and PL (d) is average path loss at distance d.

If the antennas have a unity gain (G_t and G_r equal to one), then the path loss equations become:

$$PL = \frac{(4\pi d)^2}{\lambda^2} \tag{3.4}$$

On the logarithmic scale, the path loss is given as:

$$PL(dB) = 20\log\left(\frac{4\pi d}{\lambda}\right) \tag{3.5}$$

As, $\lambda = c/f$, where f is frequency. Now for millimeter wave, the equation becomes:

$$PL(dB) = 20\log\left(\frac{4\pi f \times 10^9}{c}\right)$$
$$PL(dB) = 20\log\left(\frac{4\pi df \times 10^9}{3\times 10^8}\right) \tag{3.6}$$
$$PL(dB) = 20\log\left(\frac{4\pi}{3}\right) + 20\log f + 20\log d$$
$$PL(dB) = 32.44 + 20\log f + 20\log d$$

3.1.2 CI path model

The CI free space reference distance path loss model is one of the most common path loss models. The CI model can be used to frequencies above and below 6 GHz [6]. Because it requires fewer parameters, this model is simple, accurate, and superior to others. In equation below CI path loss is given.

$$PL^{CI}(f_{c,}d)[dB] = FSPL(f_c, d_o)[dB] + 10n\log_{10}\left(\frac{d}{1m}\right) + X_{\delta}^{CI} \tag{3.7}$$

Where, the separation between TX and RX is referred as d, n is the path loss exponent and $X\sigma$ is the shadow fading, which is Gaussian random variable with mean of zero and standard deviation

σ in dB, and FSPL is Friis' free space path loss with 1m reference distance [48]. Now FSPL for the GHz frequency range becomes:

$$FSPL(f_c, d_o)[dB] = 20\log_{10}\left(\frac{4\pi f_c d_o \times 10^9}{c}\right) \quad (3.8)$$

Where c is the speed of light. Then, by considering d_o =1m, we can simplify the equation (3.8). By giving d_o, $1m$ value equation becomes:

$$FSPL(f_c, 1m)[dB] = 32.44 + 20\log_{10} f_c \quad (3.9)$$

As a result, equation (3.7) can be written as:

$$PL^{CI}(f_c, d)[dB] = 32.44 + 20\log_{10} f_c + 10n\log_{10} d + X_\delta^{CI} \quad (3.10)$$

3.1.3 FI model

The FI path loss model is another type of path loss model. For the WINNERII Project and 3GPP channel models, FI is one of the propagation models used in channel standardization [49]. This model is sometimes referred to as the alpha-beta model. The FI model can be expressed as:

$$PL[dB] = \alpha + 10\beta\log_{10}(d) + x_\delta \quad (3.11)$$

Here α is known as the intercept in dB, β is the slope of the line that characterizes the loss distance dependence, and x_δ is the shadow fading which is Gaussian random variable with mean of zero and standard deviation σ in dB [50].

In both LOS and NLOS scenarios, the close-in free space reference distance model and the floating intercept model can be used to specify for mmWave channels [51].

3.1.4 Dual slope model

The single-slope path loss model frequently fails to account for PLE dependency on the physical environment in dense and mmWave capable network. These restriction lead to the consideration of dual slope path loss model [52]. A dual-slope path loss model with a break-point distance given as:

$$
\begin{aligned}
&P_{LDS}[dB] = PL + 10\beta \log_{10} d + X_{\delta}, \\
&d \le d_{bp} \\
&P_{LDS}[dB] = PL + 10\beta_1 \log_{10} d_{bp} + 10\beta_2 \log_{10} \frac{d}{d_{bp}} + X_{\delta}, \\
&d > d_{bp}
\end{aligned}
\tag{3.12}
$$

Here, d_{bp} is the breakpoint distance, PL is referred as a path loss model for reference distance of 1m, $\beta 1$ and $\beta 2$ represents the path loss exponent (PLE) before and after the breakpoint distance, d is the distance between TX and RX, and X_{δ} is the shadow fading which is a Gaussian random variable with a mean of zero and standard deviation σ in dB.

3.1.5 ABG model

The ABG model is a multi-frequency path loss model with a large scale [53]. It is a frequency and distance depended model. The ABG model can be written as:

$$PL^{ABG}(f,d)[dB] = 10\alpha \log_{10}(d) + \beta + \gamma 10 \log_{10}(f) + X_{\delta}^{ABG} \tag{3.13}$$

where α indicates the slope of path loss with distance, which captures how the PL increase as the transmit-receive distance (in meters) increases, β is the floating offset value in dB, which is an optimized offset parameter, and γ models the frequency dependence of path loss, where f is carrier frequency in GHz, and X_{δ}^{ABG} symbolizes zero mean Gaussian random variable with Standard deviation of δ in dB. Furthermore, α β and γ are optimized from closed-form solutions that minimize the standard deviation of shadow fading. The ABG model is solved via MMSE to minimize δ by simultaneously solving for α , β and γ .

3.1.6 Two ray model path loss model

A two-ray ray tracing model is the simplest type of ray tracing model, in which the received signal is accompanied by a ground reflected wave. There are two received signals in this models, as shown in figure 3.2: one is a LOS signal and the other is an indirect component of the transmitted signal reflected from the ground. Reflected ground signals can either interfere constructively or destructively at the receiver end [54].

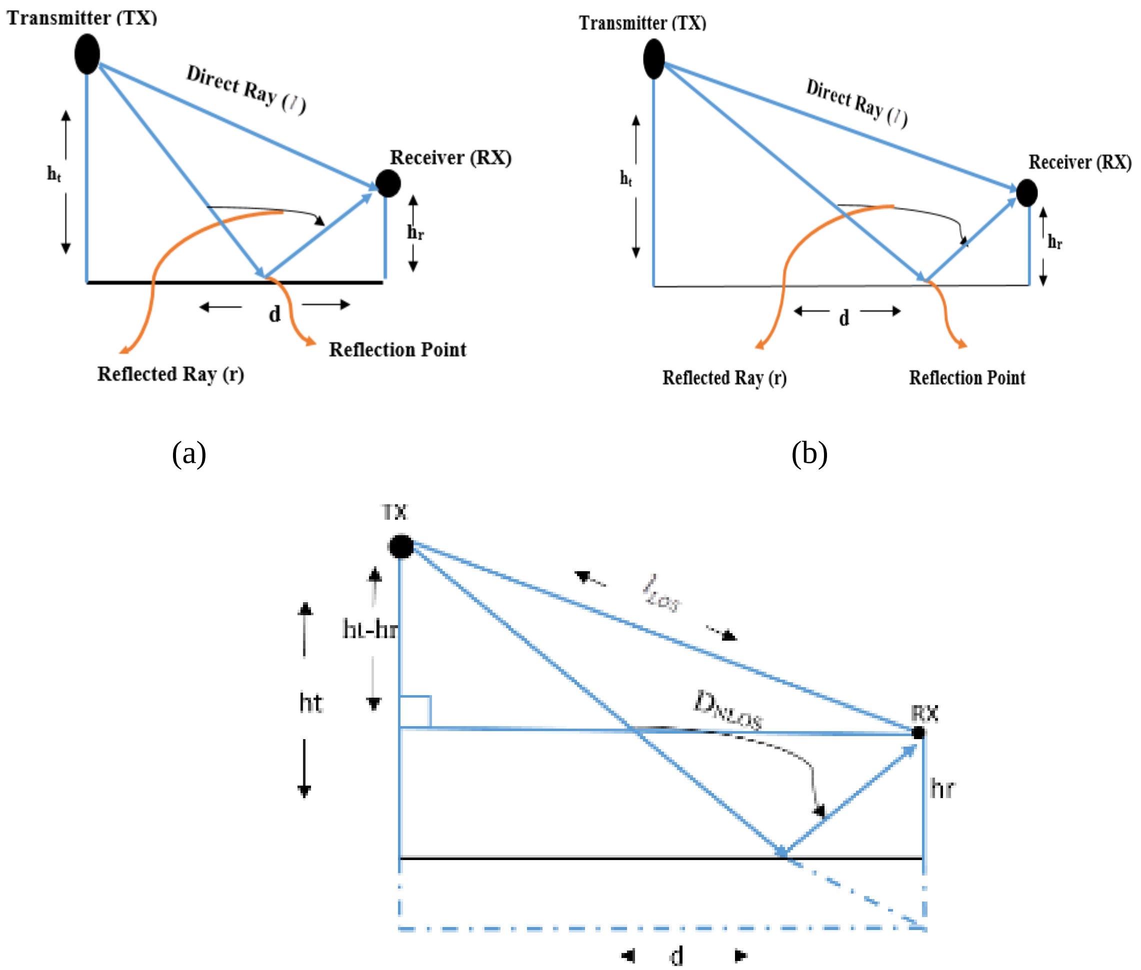

(a) (b)

(c)

Figure 3.2: Two ray ground reflection model: direct and reflected propagation path

The total received power can be written as:

$$P_R = P_T G\left(\frac{\lambda}{4\pi}\right)^2 \times \left\{\frac{l}{d} + \Gamma(\psi)\frac{e^{-j\Delta\phi}}{r}\right\}^2 \tag{3.14}$$

where P_R is the received power , P_T is transmitted power, G is the antenna gain, λ is the wavelength, d is the direct length between transmitter and receiver, Γ refers to the Fresnel Reflection Coefficient which accounts for the reflections through the obstacles, ψ is known as gazing angle, l is the direct path length, r is reflected path length and $\Delta\phi$ is the phase difference between two waves [55]. Phase difference can be expressed as:

$$\Delta\phi = \frac{2\pi(r-1)}{\lambda} \tag{3.15}$$

After obtaining the received power, the path loss can be calculated using the formula below:

$$PL[dB] = 10\log(\frac{P_T}{P_R}) \tag{3.16}$$

As a result, the path loss in the two-ray model becomes:

$$PL_{2ray} = \left(\frac{1}{\left(20\log_{10}\left[\left(\frac{\lambda}{4\pi d}\right) + \Gamma(\psi)e^{-j\Delta\phi}\right]\right)} \right) \tag{3.17}$$

When the reflection coefficient's magnitude and phase are close to one and 180, respectively, the 2-ray model can be expressed as [56]:

$$PL_{2ray} = \left(\frac{1}{\left(20\log_{10}\left[\left(\frac{\lambda}{4\pi d}\right)\left\{2\sin\left(\frac{2\pi h_t h_r}{\lambda d}\right)\right\}\right]\right)} \right) \tag{3.18}$$

Where h_t *and* h_r are transmitter and receiver height respectively. Since TX and RX are fixed, the deterministic time variations are not included and the delays for multiple signal paths are also fixed.

From figure 3.2.c using Pythagoras' theorem, the distance of LOS and NLOS is calculated as follows:

$$\begin{aligned} {l_{LOS}}^2 &= (h_t - h_r)^2 + (d)^2 \\ l_{LOS} &= \sqrt{\left((h_t - h_r)^2 + (d)^2\right)} \end{aligned} \tag{3.19}$$

For NLOS the path loss distance can be expressed as:

$$D_{NLOS}^2 = (h_t + h_r)^2 + (d)^2$$
$$D_{LOS} = \sqrt{\left((h_t + h_r)^2 + (d)^2\right)} \quad (3.20)$$

- **Influence of Fresnel zone**

Figure 3.2 (a) and (b) demonstrate a two-ray propagation situation. As seen in the figures, the RX gradually travels away from the TX. When the TX moves away from the RX, the first Fresnel zone radius increases to some point that it becomes tangent to the ground, resulting in the break point p, which is tangent to the ground and the Fresnel zone, as shown in figure 3.3.

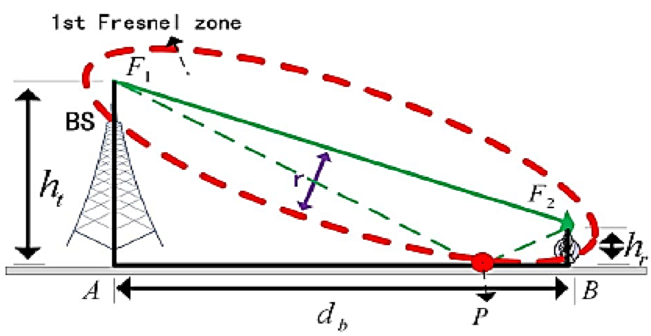

Figure 3.3: Two ray propagation scenario: with tangent point to the ground and Fresnel zone [57]

From the first Fresnel zone the break point distance can be expressed as [58]:

$$d_b = \frac{4h_t h_r}{\lambda} \quad (3.21)$$

Where h_t and h_r are height of transmitter and receiver respectively and λ is wavelength.

From equation 3.20 and 3.21, the break point distance related to path loss distance is as follows:

$$D_{NLOS}^2 = (h_t + h_r)^2 + (d)^2$$
$$D_{NLOS}^2 = ht(h_t + h_r) + h_r(h_t + h_r) + (d)^2$$
$$D_{NLOS}^2 = (h_t)^2 + h_t h_r + h_r h_t + (h_r)^2 + (d)^2 \quad (3.22)$$
$$D_{NLOS}^2 = (h_t)^2 + 2h_t h_r + (h_r)^2 + (d)^2$$

To relate path loss distance with break point distance, replace $2h_t h_r$ by d_b, then the equation can be written as:

$$D_{NLOS}^2 = (h_t)^2 + 2h_t h_r + (h_r)^2 + (d)^2$$
$$d_b = \frac{4h_t h_r}{\lambda} \quad (3.23)$$
$$d_b * \lambda = 4h_t h_r$$

Then divide $d_b * \lambda$ by two, the equation becomes:

$$\frac{d_b * \lambda}{2} = 2h_t h_r \quad (3.24)$$

Replace $2h_t h_r$ by $\frac{d_b * \lambda}{2}$ then, equation of the path loss distance expressed as follow:

$$D_{NLOS}^2 = (h_t)^2 + \frac{d_b * \lambda}{2} + (h_r)^2 + (d)^2 \quad (3.25)$$

Where h_t, h_r, d, d_b, λ denotes height of transmitter, height of receiver, separation distance between TX and RX, break point distance and wave length respectively.

By substituting equation 3.21 into equation 3.5, we derive an equation to relate the breakpoint with path loss, as follows:

$$PL(dB) = 20\log\left(\frac{4\pi d}{\lambda}\right)$$
$$d_b = 4\frac{h_t h_r}{\lambda} \quad (3.26)$$
$$\lambda = 4\frac{h_t h_r}{d_b}$$

Substitute λ in to L_P, then the equation become:

$$PL(dB) = 20\log\left(\frac{\pi d d_b}{h_t h_r}\right) \quad (3.27)$$

Table 3.1: Simulation in put parameter

Input parameters	**Value**
Carrier frequency	38/ 60/ 73 GHz
Transmit power	30 dBm
RF Bandwidth	800 MHz
Scenario	UMi
Environment	LOS/NLOS
Height of transmitter	1 m
Height of receiver	0.5 m
TX-RX separation	10-500 m
Number of RX locations	10
TX array Type, N_t	ULA,2,64
RX array Type, N_r	ULA,2,16
TX and RX antenna Spacing	0.5 λ
Azimuth and elevation HPBW for TX and RX	10^0

CHAPTER FOUR

4 RESULT AND DISCUSSION

In this section, simulation results are shown for the indoor environment at different mmWave bands and Sub 6 GHz. Different path loss models with respect to distances and breakpoint distances were analyzed to enhance the received power and throughput. The directional PDP at 38 and 73 GHz was also analyzed. The results are simulated using MATLAB and NYUSIM software. We used NYUSIM to simulate directional PDP for both 38 GHz and 73 GHz with 2x2 and 64x16 antenna configurations with 10 RX random locations. To handle massive indoor communication networks, 800MHz RF bandwidth is used. The simulation environment considers UMi for indoor environments in LOS and NLOS scenarios, with a distance between the TX and RX antenna of 10 m to 500 m and a transmission power of 30 dBm. While the distance for the directional power delay profile is between 60 m and 69 m. The TX and RX antenna spacing were considered at 0.5 λ. Both the transmitter and receiver have HPBW of 10 degree for azimuth and elevation.

4.1 Free space path loss model at both mmWave bands and sub 6 GHz

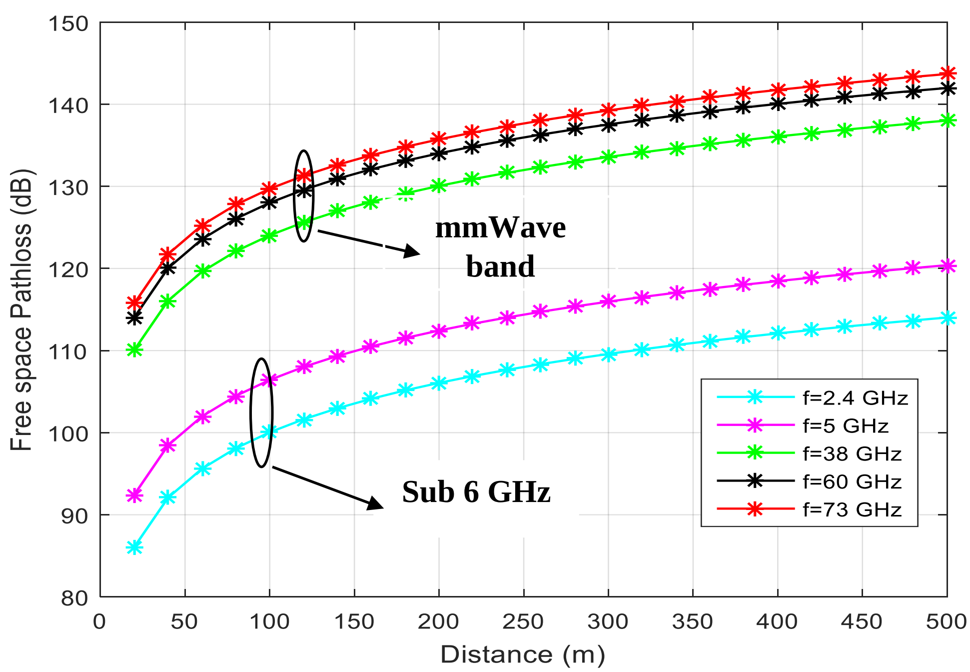

Figure 4.1: Free Path loss vs. distance

The relationship between separation distance TX-RX and path loss of free space is shown in figure 4.1 for different carrier frequencies. As the distance increases, the path loss also increases for all frequencies. Also, when the distance is doubled, the path loss is increased by 6 dB at each carrier frequency. Hence, the received signal power decreased. Furthermore, when comparing the sub-6 GHz and mmWave bands, the path loss at mmWave bands is much higher than at sub-6 GHz due to the short wave length of mmWave, which is easily obstructed.

Table 4.1: Frequency, received signal power, free space path loss

Frequency (GHz)	**Path loss (dB)**	**Received signal power (dBm)**
2.4	76.3	-46.3
5	82.7	-52.7
38	100.3	-70.3
60	104.3	-74.3
73	106	-76

For a separation distance of 65 m and a transmit power of 30 dBm, table 4.1 shows the effect of increasing carrier frequency on path loss and received signal power. The path loss increases from 76.3 dB to 106 dB as we move from sub 6 GHz (2.4 GHz) to mmWave (73 GHz), and the received signal power decreases from -46.3 dBm to -76 dBm.

4.2 Plotting of two ray path loss model at mmWave bands

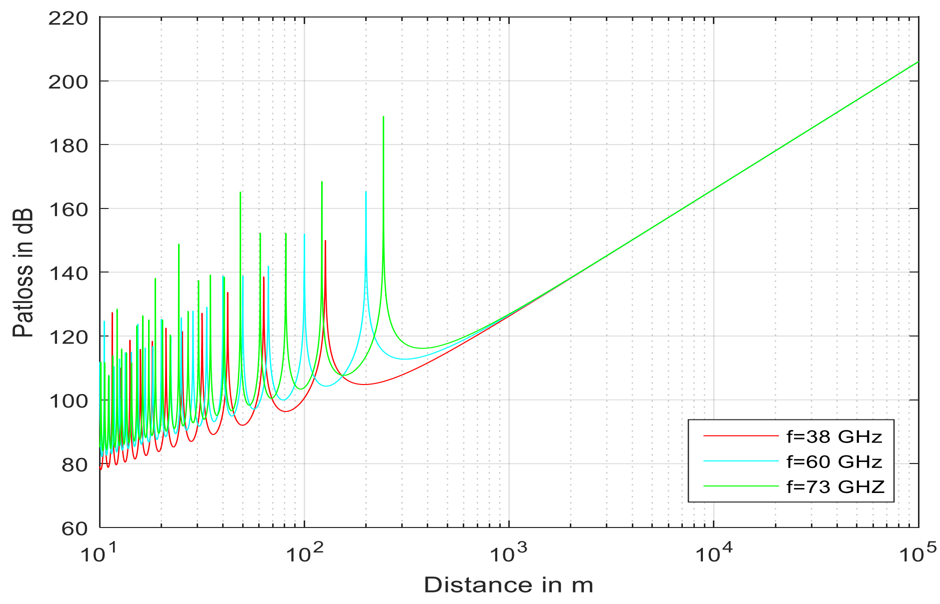

Figure 4.2: Two ray path loss vs. distance

The relationship between two ray path loss with transmitter-receiver separation distance for 38, 60, and 73 GHz, with the height of the transmitter at 1m and the height of the receiver at 0.5 m, is illustrated in figure 4.2. As the distance between the transmitter-receiver increases due to the movement of the user away from the transmitter, the path loss in two rays increases, reducing the received signal power for each frequency. The path loss takes the shape of a sinusoidal wave. These waves continue until they reach a certain point. After that point, only the path loss at 73 GHz increases linearly with distance.

4.3 CI path loss model for mmWave bands and sub 6 GHz

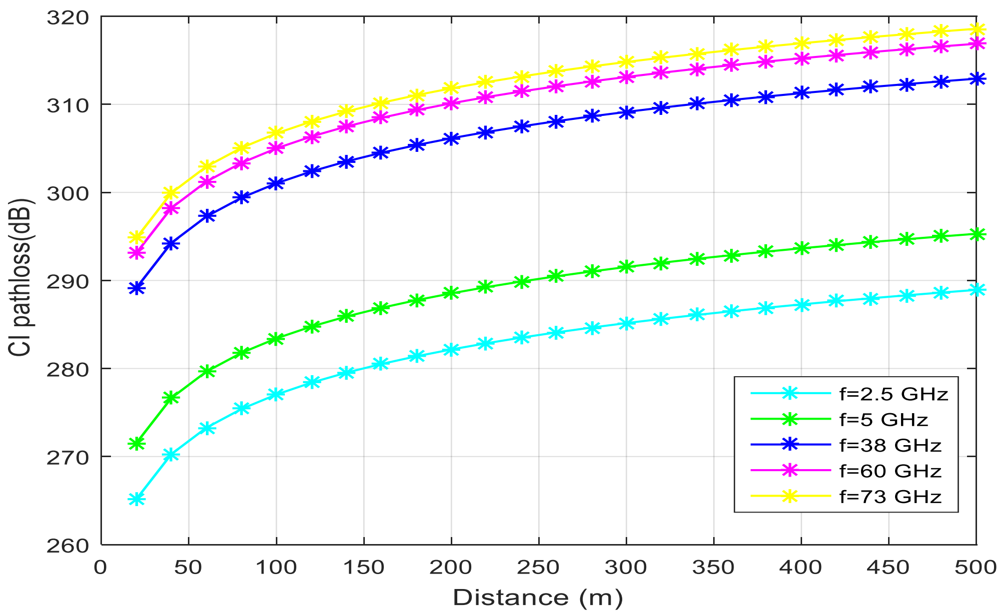

Figure 4.3: CI path loss vs. distance

The relationship between CI path loss and distance at sub 6 GHz and mmWave frequencies is shown in figure 4.3. When the separation distance between TX-RX increases, the CI path loss also increases for each frequency.

Table 4.2: Frequency, received signal power, CI path loss

Frequency (GHz)	**Path loss (dB)**	**Received signal power (dBm)**
2.4	259.3	-229.3
5	265.7	-235.7
38	283.3	-253.3
60	287.3	-257.3
73	289	-259

Table 4.1 demonstrates the effect of raising the carrier frequency from sub 6 GHz to mmWave bands on CI path loss and received signal power for a separation distance of 65 m and a transmit power of 30 dBm. The path loss increases from 259 dB to 289 dB as the frequency increases from 2.4 GHz to 73 GHz, whereas the received signal power decreases from -229.3 dBm to -259 dBm.

4.4 Comparing CI and free space path loss model for mmWave bands

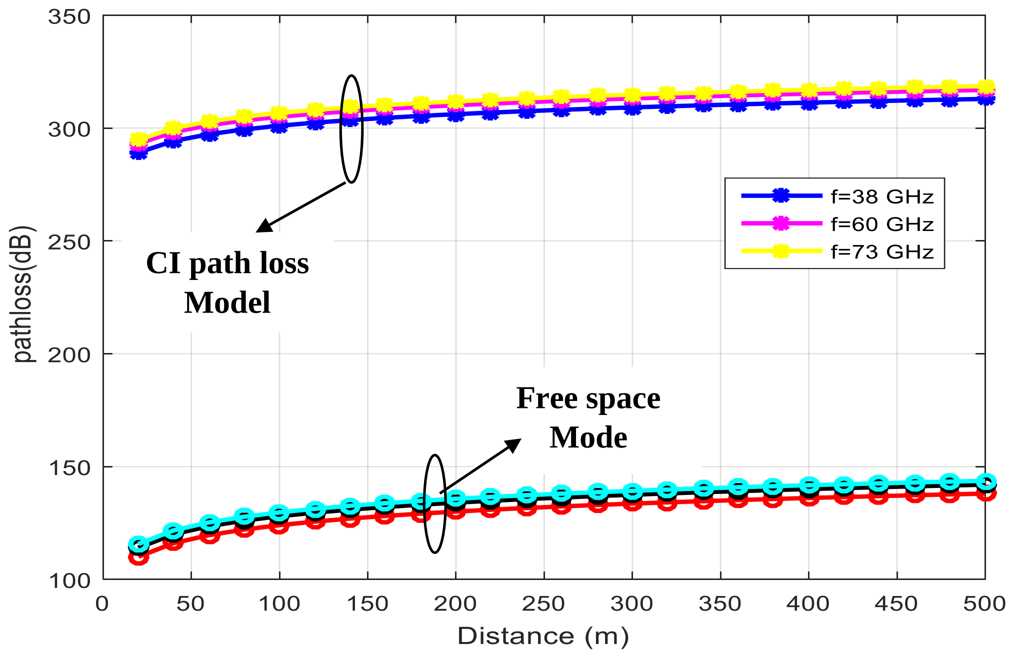

Figure 4.4: Path loss vs. distance for CI and free space path loss model

The path loss and distance relationships for both free space and the CI model at 38, 60, and 73 GHz are illustrated in figure 4.4. As shown in the figure, the path loss of the free space model is lower than the CI model, because free space does not consider the effect of shadowing and reflection. Whereas the CI model considers all shadowing and reflection effects between the transmitter and receiver, which decrease the received signal.

4.5 Plotting of free space path loss with break point distance for different heights of transmitter

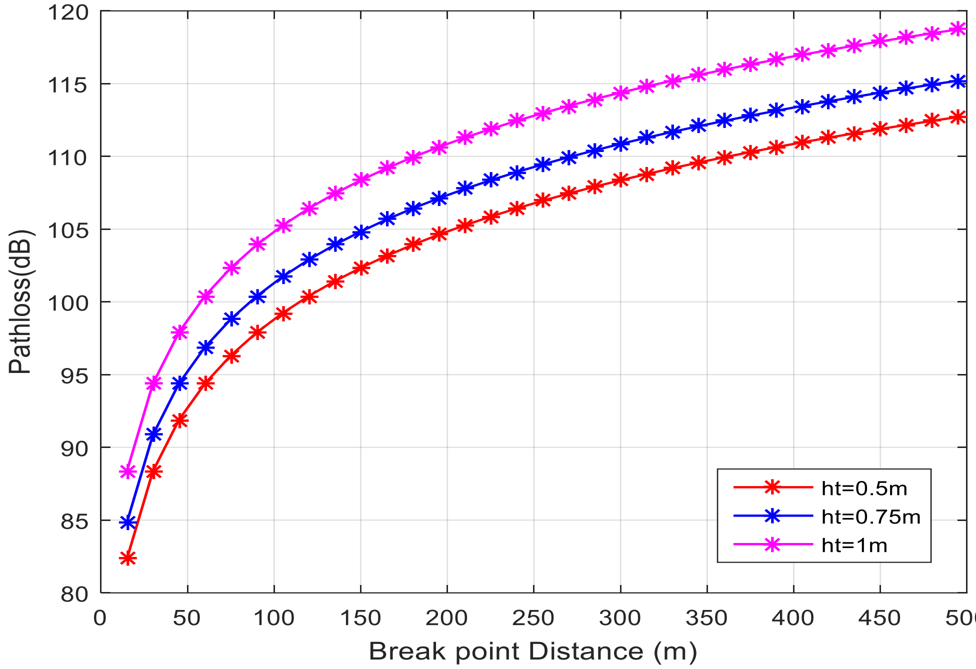

Figure 4.5: Path loss vs. break point distance

Figure 4.5 shows the relationship between free space path loss and break point distance for different heights of transmitter at 0.5 m height of receiver and 500 m separation distance. For each height of transmitter, the path loss increases as the break point distance increases. The term "break point" refers to the point at which a direct signal is reflected. The path loss increases from 82.34 dB to 88.36 dB and from 112.7 to 118 dB at 15 m and 495 m break point distances, respectively, as the transmitter height doubles. Therefore, we conclude that when the break point is near the transmitter, the received signal power is larger than the break point at the cell edge.

4.6 Plotting of break point distance with frequency for different heights of transmitter

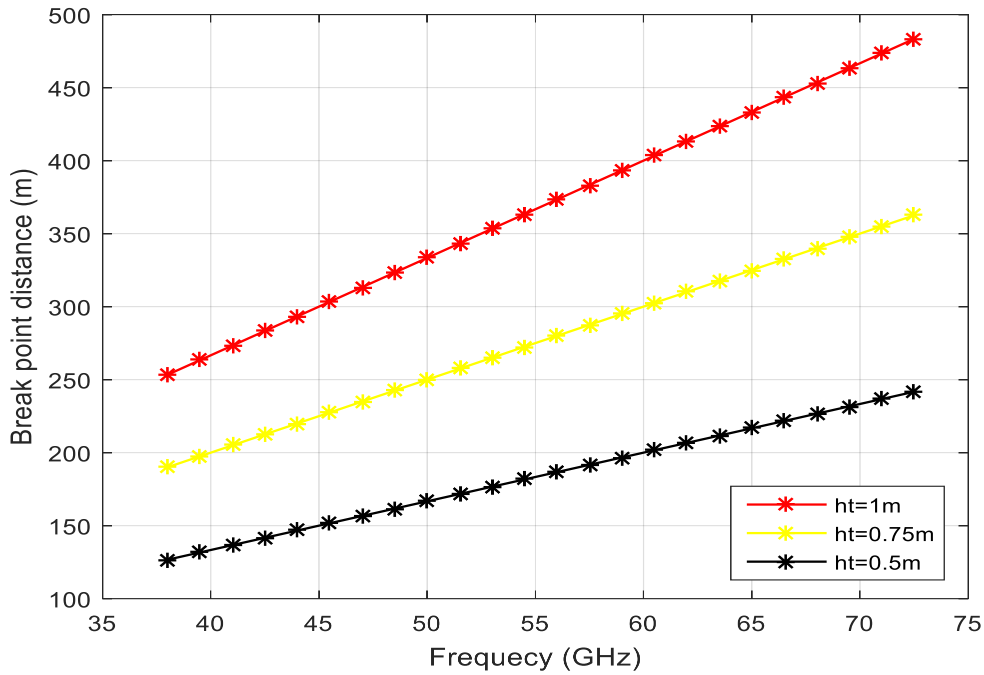

Figure 4.6: Break point distance vs. frequency

The effect of changing the height of the transmitter with a fixed receiver height (hr=0.5 m) on the break point distance as a function of frequency is shown in figure 4.6. Break point distance increases as carrier frequencies increase. With the increment of transmitter height, the break point distance also increases at each carrier frequency, which leads to an increase in path loss distance. As a result, the received signal power is reduced.

Table 4.3: Frequency, height of TX, break point and path loss distance

Frequency (GHz)	**Height of TX (m)**	**Db (m)**	**Path loss distance (m)**
38	0.5	126.7	500.0007
	0.75	190	500.0014
	1	253.3	500.0022
60	0.5	200	500.0007
	0.75	300	500.0014
	1	400	500.0022
73	0.5	241.7	500.0007
	0.75	362.5	500.0014
	1	483.1	500.0022

Table 4.3 shows the effect of transmitter height on carrier frequencies of 38, 60, and 73 GHz with a separation distance of 500 m and a receiver height of 0.5 m. When the height of the transmitter is increased from 0.5 to 1 meter, the break point distance doubles and the path loss distance increases from 500.0007 to 500.0022 m for all frequencies.

Using the MATLAB-based NYUSIM simulator, we examined the directional PDP with the strongest power at 38 and 73, using 2x2 and 64x16 antenna configurations. The impulse response of a channel model is explained by PDP, which characterizes the channel's temporal characteristics. Furthermore, a PDP describes how a signal is received at the receiver end with variable signal power as it travels through a multipath channel with increasing propagation time.

4.7 Comparing directional PDP for LOS and NLOS at 28 and 73 GHz using a 2x2 antenna configuration

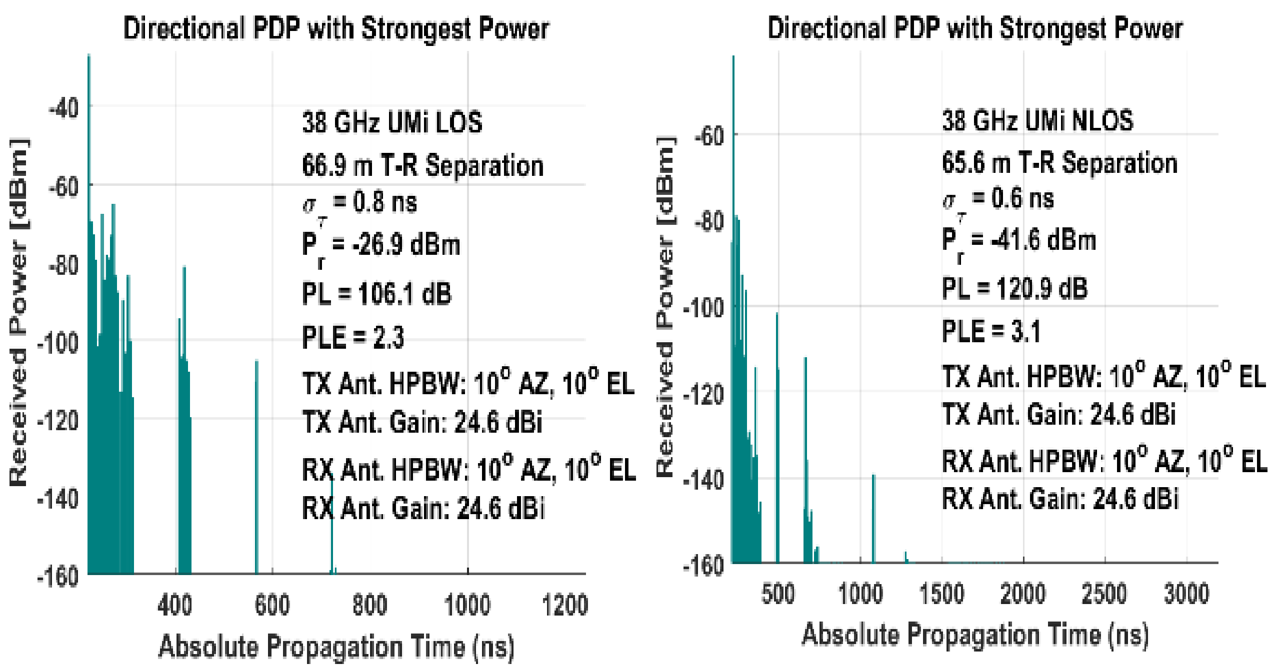

(a) LOS directional PDP (b) NLOS directional PDP

Figure 4.7: Directional PDP at 38 GHz for both LOS and NLOS environment with 2x2 antenna configuration

The Directional PDP with the strongest power is illustrated in figure 4.7. The figures show the received power vs. propagation time, as well as received signal power, path loss, PLE, RMS delay spread, and antenna characteristics for both LOS and NLOS conditions at 38 GHz for the ULA

2X2 antenna configuration. As seen in figure 4.7.a, the received power decreases exponentially as propagation time increases, and the inter-cluster gap widens. The term inter-cluster gap refers to the short time the transmitted signal takes from reflection and scattering to reach the receiver end. Figure 4.7.b shows received power decreasing exponentially with increasing propagation time, similar to figure 4.7.a. Therefore, we conclude that the received power has an inverse relationship with the propagation time for both LOS and NLOS PDPs with the strongest power. When comparing figures 4.7.a and 4.7.b, the received power of LOS is higher than NLOS. Additionally, the propagation time of NLOS is longer than that of LOS, as indicated in the figures.

Table 4.4: Directional power delay characteristics at 38 GHz for 2x2 antenna configuration

Frequency (GHz)	**Scenario**	**TX-RX Separation (m)**	σ_τ **(ns)**	P_r **(dBm)**	**PL (dB)**	**PLE**
38	LOS	66.9	0.8	-26.9	106.1	2.3
	NLOS	65.6	0.6	-41.6	120.9	3.1

Table 4.4 shows power delay statistics with RMS delay spread, received power, path loss, and PLE for both LOS and NLOS directional PDP at 38 GHz using a 2X2 antenna configuration. In the LOS scenario, the received signal power is -26.9 dBm with PLE 2.3, whereas in NLOS it is -41.6 dBm with PLE 3.1. As a result, the received signal in the LOS scenario is larger than in the NLOS scenario, since in the NLOS scenario, there are many obstacles between the transmitter and the users, causing the transmitted signal to go through a multipath channel, reducing the received signal power. Furthermore, when comparing the PLE for both LOS and NLOS scenarios to the PLE for free space, the PLE for LOS is nearly equal to the PLE for free space, but the PLE for NLOS is more than it.

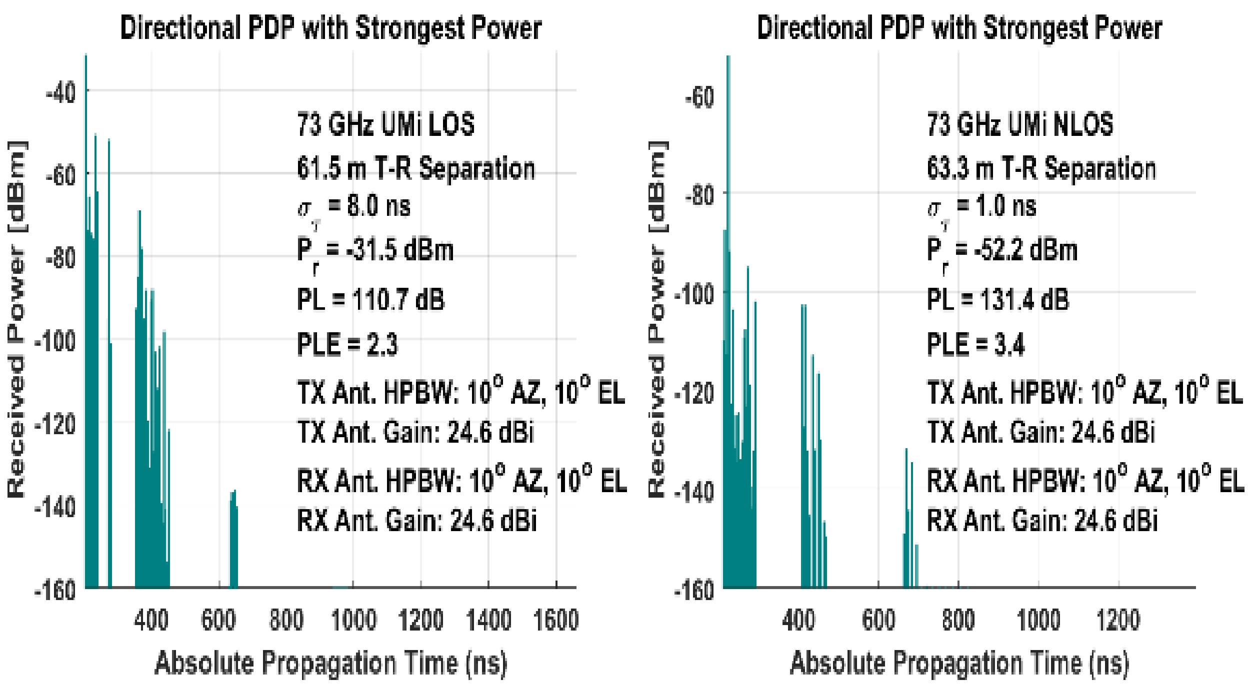

(a) LOS directional PDP (b) NLOS directional PDP

Figure 4.8: Directional PDP at 73 GHz for both LOS and NLOS environment with 2x2 antenna configuration

Figure 4.8 shows the directional PDP with the strongest power. The figures show received power vs. propagation time, as well as received signal power, path loss, PLE, RMS delay spread, and antenna characteristics for both LOS and NLOS conditions at 73 GHz for the ULA 2X2 antenna configuration. As seen in both figures 4.8.a and 4.8.b, the received power decreases exponentially with increasing propagation time. The received power has an inverse relationship with the propagation time interval for both the LOS and NLOS PDPs with the strongest power.

Table 4.5: Directional power delay characteristics at 73 GHz for 2x2 antenna configuration

Frequency (GHz)	Scenario	TX-RX Separation (m)	σ_τ (ns)	P_r (dBm)	PL (dB)	PLE
73	LOS	61.5	8	-31.5	110.7	2.3
	NLOS	63.3	1	-52.2	131.4	3.4

Directional power delay with RMS delay spread, received power, path loss and PLE for both LOS and NLOS directional PDP at 73 GHz using a 2X2 antenna configuration are illustrated in table 4.5. In the LOS scenario, the received signal power is -31.5 dBm with PLE 2.3, whereas in NLOS it is 52.2 dBm with PLE 3.4. Therefore, the received signal in the LOS scenario is higher than in the NLOS, like that of 38 GHz. When comparing the received signal power of 38 GHz to 73 GHz, the received signal power of 38 GHz is greater than 73 GHz for both LOS and NLOS, with path loss of 106.1 and 120.9, respectively. At 73 GHz, the path loss for LOS and NLOS is 110.7 and 131.4, respectively. The large path loss at 73 GHz is due to the fact that when carrier frequencies increase, path loss increases as well, reducing the received signal power.

4.8 Comparing directional PDP for LOS and NLOS at 38 and 73 GHz using 64x16 antenna configuration

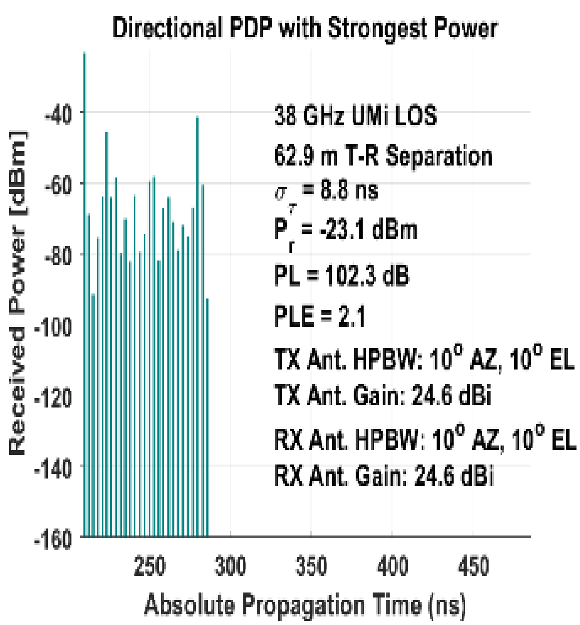

(a) LOS directional PDP

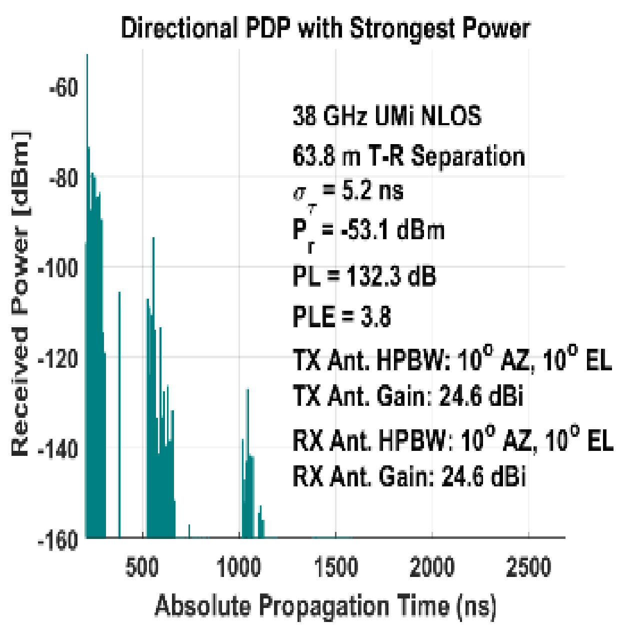

(b) NLOS directional PDP

Figure 4.9: Directional power delay profile at 38 GHz for both LOS and NLOS environment with 64x16 antenna configuration

The Directional PDP with the strongest power is illustrated in figure 4.9. The figures show received power vs. propagation time, as well as received signal power, path loss, PLE, RMS delay spread, and antenna characteristics for both LOS and NLOS conditions at 38 GHz for the ULA 64X16 antenna configuration. As seen in figure 4.9.a, the received power is high within a short propagation time. Figure 4.9.b shows received power decreasing exponentially with increasing propagation time. The propagation time in LOS is short when compared to figures 4.9.a and 4.9.b and also figure 4.8. Which means that the receiver received the best signal power in a short period of time, due to the large number of antennas used. Additionally, the inter-cluster gap is very small.

Table 4.6: Directional power delay characteristics at 38 GHz for 64x16 antenna configuration

Frequency (GHz)	Scenario	TX-RX Separation (m)	σ_τ (ns)	P_r (dBm)	PL (dB)	PLE
38	LOS	62.9	8.8	-23.1	102.3	2.1
	NLOS	63.8	5.2	-53.1	132.2	3.8

Table 4.6 illustrates power delay with RMS delay spread, received power, and path loss for both LOS and NLOS directional PDP at 38 GHz for the 64X16 antenna configuration. In the LOS scenario, the received signal power is –23.1 dBm with PLE 2.1, whereas in NLOS it is-53.1 dBm with PLE. When comparing the PLE for both LOS and NLOS scenarios with the free space PLE, the PLE for LOS is nearly equal to free space, but the NLOS PLE is approximately 4. The received signal obtained at 38 GHz using 64X16 is greater than 2x2 for LOS, it improved by 3.8 dBm. However, for NLOS, the received signal using 2x2 is larger than 64x16 because in this scenario there are multipath effects that reduce the received signal power.

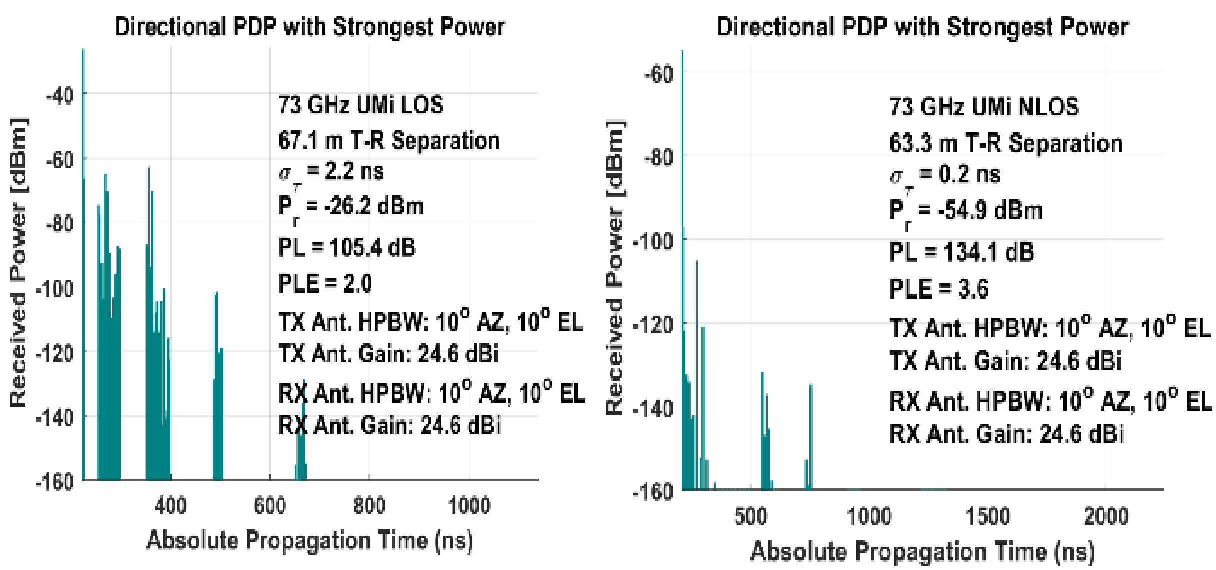

(a) LOS directional PDP (b) NLOS directional PDP

Figure 4.10: Directional power delay profile at 73 GHz for both LOS and NLOS environment with 64x16 antenna configuration

The Directional PDP with the strongest power is illustrated in figure 4.10. The figures show received power vs. propagation time, as well as received signal power, path loss, PLE, RMS delay spread, and antenna characteristics for both LOS and NLOS conditions at 73 GHz for the ULA 64X16 antenna configuration. The received power decreases exponentially as propagation time increases, as seen in figures 4.9.a and 4.9.b. When we compare figure 4.10.a with figure 4.10.b and figure 4.9, the received signal power in LOS is large. Which means that the receiver received the best signal power of the two, due to the large number of antennas used.

Table 4.7: Directional power delay characteristics at 73 GHz for 64x16 antenna configuration

Frequency (GHz)	**Scenario**	**TX-RX Separation (m)**	σ_τ **(ns)**	P_r **(dBm)**	**PL (dB)**	**PLE**
73	LOS	67.1	2.2	-26.2	105.4	2
	NLOS	63.3	0.2	-54.9	134.1	3.6

Table 4.7 illustrates power delay statistics with RMS delay spread, received power, path loss, and PLE for both LOS and NLOS for directional PDP at 73 GHz for a 64X16 antenna configuration. In the LOS scenario, the received signal power is -26.2 dBm with PLE 2.3, whereas in NLOS it is -54.1 dBm with PLE 3.6. When comparing the PLE for both the LOS and NLOS scenarios to the PLE for free space, the LOS PLE equals free space, while the NLOS PLE exceeds it. The received signal power obtained at 73 GHz using 64X16 is greater than 2x2 for LOS and improved by 5.3 dBm. However, for NLOS, the received signal using 2x2 is larger than 64x16, like that of 38 GHz. Therefore, we conclude that increasing the number of antennas enhances the received signal power for frequencies in LOS, whereas in the NLOS scenario, it decreases the received signal power.

5 CONCLUSION AND RECOMMENDATION

5.1 Conclusion

The vast amount of unused frequency resources in the mmWave spectrum is being considered as one of the primary solutions to indoor communication network congestion. Hence, the frequency bands in mmWave offer larger bandwidths for wireless indoor communication systems. Despite the fact that a huge bandwidth is employed, mmWave technology suffers from path loss, atmospheric attenuation, building penetration loss, diffuse scattering from rough materials, shadowing, and reflection loss. As a result, the transmitted signal power and throughput are decreased. In this thesis, path loss is considered at 38 GHz, 60 GHz, 73 GHz and sub 6 GHz using CI, two-ray and free space path loss models.

The results have shown that the path loss increases with an increase in separation distance and carrier frequency. The path loss in the CI model is larger than that of two rays and free space, because it considers all the shadowing and reflection effects between transmitter and receiver. Despite the fact of high path loss, the CI model is the most suitable for an indoor communication network. Additionally, the relationship between breakpoint distance and path loss have been examined. Path loss increases as the breakpoint distance and carrier frequency increase. In addition, when the break point distance is greater than the separation distance, the PLE is larger than in free space PLE.

Finally, the directional power delay profile with the strongest power at 38 and 73 GHz for both LOS and NLOS environments using 2x2 and 64x16 antenna configurations has been examined. In both antenna configurations, the received signal power in LOS at 38 GHz and 73 GHz is greater than in NLOS. Furthermore, for both carrier frequencies, the received signal power in a 64x16 antenna configuration is larger than in a 2x2 configuration. Therefore, we conclude that increasing the number of antennas used at the transmitter increases the received signal power and throughput. However, increasing the number of antennas increases the received power of the LOS scenario, not the NLOS scenario. Hence, in 64x16 for both 38 and 73 GHz in NLOS, the received power is smaller than in the 2x2 NLOS scenario. Moreover, the PLE is nearly equal to the free space PLE in all LOS scenarios, whereas in NLOS it is greater than in free space.

5.2 Recommendation

In this thesis, the performance of the CI, free space and two ray path loss models with respect to separation distance and break point distance were analyzed. The received signal power and throughput are enhanced by minimizing the path loss for the used carrier frequencies by using a large number of antennas at BSs. In the future, using different polarization techniques, antenna configurations (URA), and other techniques called beam-forming are recommended to be done to enhance the received signal power and throughput in the given area for different mmWave frequencies by considering other impairments of the mmWave indoor communication network.

REFERENCES

[1] Z. Lin, X. Du, H. Chen, B. Ai, Z. Chen, and D. Wu (2019), “Millimeter-Wave Propagation Modeling and Measurements for 5G Mobile Networks,” no. February, pp. 72–77.

[2] M. Series (2015), “IMT Vision--Framework and overall objectives of the future development of IMT for 2020 and beyond,” *Recomm. ITU*, vol. 2083.

[3] S. Mumtaz, J. Rodriguez, and L. Dai (2016), “MmWave massive MIMO: a paradigm for 5G,” Academic Press.

[4] T. E. Bogale and L. B. Le (2016), “Massive MIMO and mmWave for 5G wireless HetNet: Potential benefits and challenges,” *IEEE Veh. Technol. Mag.*, vol. 11, no. 1, pp. 64–75.

[5] J. G. Andrews *et al.* (2014), “What will 5G be?,” *IEEE J. Sel. areas Commun.*, vol. 32, no. 6, pp. 1065–1082.

[6] Z. Pi and F. Khan (2011), “An introduction to millimeter-wave mobile broadband systems,” *IEEE Commun. Mag.*, vol. 49, no. 6, pp. 101–107.

[7] F. Rusek *et al.* (2012), “Scaling up MIMO: Opportunities and challenges with very large arrays,” *IEEE Signal Process. Mag.*, vol. 30, no. 1, pp. 40–60.

[8] L. Wei, R. Q. Hu, Y. Qian, and G. Wu (2014), “Key elements to enable millimeter wave communications for 5G wireless systems,” *IEEE Wirel. Commun.*, vol. 21, no. 6, pp. 136–143.

[9] M. A. Mou (2019), “Indoor mmWave Statistical Channel Model at V-Band for 5G Networks,” pp. 26–28.

[10] F. Al-Ogaili and R. M. Shubair (2016), “Millimeter-wave mobile communications for 5G: Challenges and opportunities,” in *2016 IEEE International Symposium on Antennas and Propagation (APSURSI)*, pp. 1003–1004.

[11] A. M. Al-samman, T. Abd, M. Hadri, and S. A. Al-gailani (2018), “Millimeter-wave propagation measurements and models at 28 GHz and 38 GHz in a dining room for 5G wireless networks,” *Measurement*, vol. 130, pp. 71–81.

[12] Y. Niu, Y. Li, D. Jin, L. Su, and A. V Vasilakos (2015), “A survey of millimeter wave communications (mmWave) for 5G: opportunities and challenges,” *Wirel. networks*, vol. 21, no. 8, pp. 2657–2676.

[13] G. Ancans, V. Bobrovs, A. Ancans, and D. Kalibatiene (2017), “Spectrum considerations for 5G mobile communication systems,” *Procedia Comput. Sci.*, vol. 104, pp. 509–516.

[14] P. Tracy (2016), "What is Mm Wave and How Does It Fit into 5G?," *Diambil dari http//www. rcrwireless. com/20160815/fundamentals/mmwave-5g-tag31-tag99*.

[15] D. T. Jangam (2013), "Mm waves role in satellite communication," *IOSR-JECE*, vol. 4, no. 4, pp. 1–4.

[16] S. Singh and M. Chawla (2017), "A Review on Millimeter Wave Communication and Effects on 5G Systems," *Iarjset*, vol. 4, no. 7, pp. 28–33.

[17] X. Ge, S. Tu, G. Mao, C.-X. Wang, and T. Han (2016), "5G ultra-dense cellular networks," *IEEE Wirel. Commun.*, vol. 23, no. 1, pp. 72–79.

[18] M. Xiao *et al.* (2017), "Millimeter Wave Communications for Future Mobile Networks," *IEEE J. Sel. Areas Commun.*, vol. 35, no. 9, pp. 1909–1935.

[19] N. K. Mallat, M. Ishtiaq, A. U. Rehman, and A. Iqbal (2020), "Millimeter-Wave in the Face of 5G Communication Potential Applications," *IETE J. Res.*, vol. 0, no. 0, pp. 1–9.

[20] 5G Americas (2020) ,"Understanding mmWave Spectrum for 5G Networks [whitepaper]" pp. 1–108.

[21] M. R. Akdeniz *et al.* (2014), "Millimeter wave channel modeling and cellular capacity evaluation," *IEEE J. Sel. areas Commun.*, vol. 32, no. 6, pp. 1164–1179.

[22] I. A. Hemadeh, K. Satyanarayana, M. El-Hajjar, and L. Hanzo (2017), "Millimeter-wave communications: Physical channel models, design considerations, antenna constructions, and link-budget," *IEEE Commun. Surv. \& Tutorials*, vol. 20, no. 2, pp. 870–913.

[23] T. S. Rappaport *et al.* (2013), "Millimeter wave mobile communications for 5G cellular: It will work!," *IEEE access*, vol. 1, pp. 335–349.

[24] Y.-P. Zhang, P. Wang, and A. Goldsmith (2015), "Rainfall effect on the performance of millimeter-wave MIMO systems," *IEEE Trans. Wirel. Commun.*, vol. 14, no. 9, pp. 4857–4866.

[25] M. Marcus and B. Pattan (2005), "Millimeter wave propagation: spectrum management implications," *IEEE Microw. Mag.*, vol. 6, no. 2, pp. 54–62.

[26] T. S. Rappaport and S. Deng (2015), "73 GHz Wideband Millimeter-Wave Foliage and Ground Reflection Measurements and Models," pp. 1238–1243.

[27] T. S. Rappaport, R. W. Heath Jr, R. C. Daniels, and J. N. Murdock (2015), *Millimeter wave wireless communications*. Pearson Education.

[28] Z. Pi and F. Khan (2011), "System design and network architecture for a millimeter-wave

mobile broadband (MMB) system," in *34th IEEE Sarnoff Symposium*, pp. 1–6.

[29] S. Rangan, T. S. Rappaport, and E. Erkip (2014), "Millimeter-wave cellular wireless networks: Potentials and challenges," *Proc. IEEE*, vol. 102, no. 3, pp. 366–385.

[30] A. N. Uwaechia and N. M. Mahyuddin (2020), "A comprehensive survey on millimeter wave communications for fifth-generation wireless networks: Feasibility and challenges," *IEEE Access*, vol. 8, pp. 62367–62414.

[31] L. Raschkowski, P. Kyösti, K. Kusume, T. Jämsä, and V. Nurmela (2015), "Deliverable D1. 4: METIS channel models," *METIS, Doc. Number ICT-317669-METIS/D1. 4*.

[32] R. J. Weiler *et al.* (2016), "Quasi-deterministic millimeter-wave channel models in MiWEBA," *EURASIP J. Wirel. Commun. Netw.*, vol. 2016, no. 1, pp. 1–16.

[33] S. Jaeckel, L. Raschkowski, K. Börner, and L. Thiele, "QuaDRiGa (2014): A 3-D multi-cell channel model with time evolution for enabling virtual field trials," *IEEE Trans. Antennas Propag.*, vol. 62, no. 6, pp. 3242–3256.

[34] R. Hasan, M. M. Mowla, M. A. Rashid, M. K. Hosain, and I. Ahmad (2019), "A Statistical Analysis of Channel Modeling for 5G mmWave Communications," *2nd Int. Conf. Electr. Comput. Commun. Eng. ECCE 2019*, pp. 7–9.

[35] H. Shokri-Ghadikolaei, L. Gkatzikis, and C. Fischione (2015), "Beam-searching and transmission scheduling in millimeter wave communications," in *2015 IEEE international conference on communications (ICC)*, pp. 1292–1297.

[36] W. Roh *et al.* (2014), "Millimeter-Wave Beamforming as an Enabling Technology for 5G Cellular," *IEEE Commun. Mag.*, vol. 52, no. 2, pp. 106–113.

[37] B. Romanous, N. Bitar, A. Imran, and H. Refai (2016), "Network densification: Challenges and opportunities in enabling 5G," *2015 IEEE 20th Int. Work. Comput. Aided Model. Des. Commun. Links Networks, CAMAD 2015*, no. I, pp. 129–134.

[38] E. Hossain and M. Hasan (2015), "IEEE Instrumentation & Measurement Magazine 5G Cellular: Key Enabling Technologies and Research Challenges," *IEEE Instrum. Meas. Mag.*, vol. 15, no. June, pp. 11–21.

[39] C. Seker, M. T. Güneser, and T. Ozturk (2018), "A review of millimeter wave communication for 5G," in *2018 2nd International Symposium on Multidisciplinary Studies and Innovative Technologies (ISMSIT)*, pp. 1–5.

[40] M. M. Abdulwahid, O. A. S. Al-ani, M. F. Mosleh, and R. A. Abd-alhmeed (2019),

"Investigation of millimeter-wave indoor propagation at different frequencies," pp. 2–8.

[41] A. M. Al-Samman *et al.* (2019), "Comparative study of indoor propagation model below and above 6 GHz for 5G wireless networks," *Electronics*, vol. 8, no. 1, p. 44.

[42] O. C. Nosiri, C. F. Umanah, C. C. Otubelu, and O. O. Okechukwu (2020), "Performance Analysis Of Millimeter-Wave Pathloss Propagation Models For 5G Network In An Indoor Environment," vol. 9, no. 1, pp. 32–38.

[43] G. R. Maccartney, S. Member, S. Deng, S. Member, and T. S. Rappaport (2016), "Indoor Office Plan Environment and Layout-Based MmWave Path Loss Models for 28 GHz and 73 GHz," pp. 0–5.

[44] D. Pimienta-del-Valle, L. Mendo, J. M. Riera, and P. Garcia-del-Pino (2020), "Indoor LOS Propagation Measurements and Modeling at 26, 32, and 39 GHz Millimeter-Wave Frequency Bands," *Electronics*, vol. 9, no. 11, p. 1867.

[45] S. Deng, M. K. Samimi, and T. S. Rappaport (2015), "28 GHz and 73 GHz Millimeter-Wave Indoor Propagation Measurements and Path Loss Models," pp. 8–12.

[46] M. B. Majed, T. A. Rahman, O. A. Aziz, M. N. Hindia, and E. Hanafi (2018), "Channel Characterization and Path Loss Modeling in Indoor Environment at 4 . 5 , 28 , and 38GHz for 5G Cellular Networks," vol. 2018.

[47] A. F. Molisch (2012), *Wireless communications*, vol. 34. John Wiley \& Sons.

[48] G. R. Maccartney, T. S. Rappaport, S. Sun, and S. Deng (2015), "Indoor office wideband millimeter-wave propagation measurements and channel models at 28 and 73 GHz for ultra-dense 5G wireless networks," *IEEE access*, vol. 3, pp. 2388–2424.

[49] L. Rubio *et al.* (2019), "Contribution to the channel path loss and time-dispersion characterization in an office environment at 26 GHz," *Electronics*, vol. 8, no. 11, p. 1261.

[50] D. Pimienta-del-Valle, S. Hernández-Sáenz, P. Sáiz-Coronado, L. Mendo, P. Garcia-del-Pino, and J. M. Riera (2019), "Indoor path loss measurements at the 5G millimeter-wave bands of 26 and 39 GHz," in *2019 13th European Conference on Antennas and Propagation (EuCAP)*, pp. 1–5.

[51] T. S. Rappaport, G. R. Maccartney, S. Member, M. K. Samimi, S. Sun, and S. Member (2015), "Wideband Millimeter-Wave Propagation Measurements and Channel Models for Future Wireless Communication System Design," vol. 6778, no. c, pp. 1–25.

[52] H. Munir, S. A. Hassan, H. Pervaiz, Q. Ni, and L. Musavian (2017), "Resource optimization

in multi-tier HetNets exploiting multi-slope path loss model," *IEEE Access*, vol. 5, pp. 8714–8726.

[53] S. Sun, G. R. MacCartney, and T. S. Rappaport (2016), "Millimeter-wave distance-dependent large-scale propagation measurements and path loss models for outdoor and indoor 5G systems," in *2016 10th European Conference on Antennas and Propagation (EuCAP)*, pp. 1–5.

[54] A. Bhuvaneshwari, R. Hemalatha, and T. Satyasavithri (2015), "Path loss prediction analysis by ray tracing approach for NLOS indoor propagation," in *2015 International Conference on Signal Processing and Communication Engineering Systems*, pp. 486–491.

[55] N. H. Ranchagoda, S. Kandeepan, M. Ding, A. Al-Hourani, and K. M. Gomez (2019), "Diversity Based Coverage Improvement for Air-to-Ground Wireless Channels," in *2019 IEEE International Conference on Wireless for Space and Extreme Environments (WiSEE)*, pp. 116–121.

[56] N. Mehrnia and M. K. Ozdemir (2019), "Ray tracing-based maritime channel analysis for millimeter radiowaves," *J. Infrared, Millimeter, Terahertz Waves*, vol. 40, no. 1, pp. 108–130.

[57] R. He *et al.* (2012), "Analysis of the Relation Between Fresnel Zone and Path Loss Exponent Based on Two-Ray Model," vol. 11, pp. 208–211.

[58] E. Zochmann, K. Guan, and M. Rupp (2017), "Two-ray models in mmWave communications," *IEEE Work. Signal Process. Adv. Wirel. Commun. SPAWC*, vol. 2017-July, pp. 1–5.

APPENDIX

```
clc;
clear all;
close all;
c=3*10^8;
hr=0.5;
ht=1;
hrv=1.45:.05:1.85;
pt=30
axis=[];
pl11=[];
pl12=[];
pl13=[];
fsl1=[];
fsl2=[];
fsl3=[];

f=2.4*1e9
f2=5*1e9
f3=38*1e9
f4=60*1e9
f5=73*1e9
d=0:20:500
lam=c/f
lam1=c/f2
lam2=c/f3
lam3=c/f4
lam4=c/f5

pl=20*log10(4*pi*d./lam)
pl1=20*log10(4*pi*d./lam1)
pl2=20*log10(4*pi*d./lam2)
pl3=20*log10(4*pi*d./lam3)
pl4=20*log10(4*pi*d./lam4)

plot(d,pl,'c-*','linewidth',1) ; hold on
plot(d,pl1,'m-*','linewidth',1);hold on
plot(d,pl2,'g-*','linewidth',1);hold on
plot(d,pl3,'k-*','linewidth',1);hold on
plot(d,pl4,'r-*','linewidth',1);
xlabel('Distance (m)');
ylabel('Free space Pathloss (dB)');
legend('f=2.4 GHz','f=5 GHz','f=38 GHz', 'f=60 GHz','f=73 GHz');
 grid
%---------------------------------------------
figure
for i=1000:5000
    d1=10^(i/1000);
    axis=[axis d1];
    fsl=((lam2/(4*3.14*d1))^2)
    fsl1=((lam3/(4*3.14*d1))^2)
   fsl2=((lam4/(4*3.14*d1))^2)

    pl4=1/(fsl*(((2*sin(2*3.14*hr*ht/(lam2*d1)))^2)));
```

```
    pl5=1/(fsl1*(((2*sin(2*3.14*hr*ht/(lam3*d1)))^2)));
    pl6=1/(fsl2*(((2*sin(2*3.14*hr*ht/(lam4*d1)))^2)));
     pl11=[pl11,10*log10(pl4)];
pl12=[pl12,10*log10(pl5)];
pl13=[pl13,10*log10(pl6)];
fsl1=[fsl1,10*log10(fsl)];
end
semilogx(axis,pl11, 'r-',axis,pl12, 'c-',axis,pl13, 'g-')
xlabel('Distance in m');
ylabel('Patloss in dB');
grid on
legend('f=38 GHz','f=60 GHz ','f=73 GHZ')
%---------------------------------------------
figure
p_L4=32.44+20*log10(f)+10*1.7*log10(d)+1.5
p_L3=32.44+20*log10(f2)+10*1.7*log10(d)+3
p_L=32.44+20*log10(f3)+10*1.7*log10(d)+3
p_L1=32.44+20*log10(f4)+10*1.7*log10(d)+3
p_L2=32.44+20*log10(f5)+10*1.7*log10(d)+3
pl=20*log10(4*pi*d./lam2)
pl1=20*log10(4*pi*d./lam3)
pl2=20*log10(4*pi*d./lam4)
plot(d,p_L4,'c-*','linewidth',1) ; hold on
plot(d,p_L3,'g-*','linewidth',1) ; hold on
plot(d,p_L,'b-*','linewidth',1) ; hold on
 plot(d,p_L1,'m-*','linewidth',1);hold on
  plot(d,p_L2,'y-*','linewidth',1);hold on

xlabel('Distance (m)');
ylabel(' CI pathloss(dB)');
legend('f=2.5 GHz','f=5 GHz','f=38 GHz','f=60 GHz','f=73 GHz');
grid
%----------------------------------------------
figure
plot(d,p_L,'b-*','linewidth',1) ; hold on
 plot(d,p_L1,'m-*','linewidth',1);hold on
  plot(d,p_L2,'y-*','linewidth',1);hold on

  plot(d,pl,'r-o','linewidth',1) ; hold on
 plot(d,pl1,'k-o','linewidth',1);hold on
  plot(d,pl2,'c-o','linewidth',1);hold on
xlabel('Distance (m)');
ylabel(' pathloss(dB)');
legend('f=38 GHz','f=60 GHz','f=73 GHz');
grid
%-----------------------------------------------------
figure
d=500;
hr1=0.5
htx=0.5
htx1=0.75
hr1=1.8
dbx=0:15:500
vv=dbx.^2
pl_db=(4*pi*d)^2.*vv/(4*ht*hr1)^2
pl_db1=(4*pi*d)^2.*vv/(4*htx1*hr1)^2
pl_db2=(4*pi*d)^2.*vv/(4*htx*hr1)^2
```

```
zz=10*log10(pl_db);
zy=10*log10(pl_db1);
zx=10*log10(pl_db2);
  plot(dbx,zz,'r-*','linewidth',1) ; hold on
  plot(dbx,zy,'b-*','linewidth',1) ; hold on
  plot(dbx,zx,'m-*','linewidth',1) ; hold on
  legend('ht=0.5','ht=0.75','ht=1')
  xlabel('Break point Distance (m)');
ylabel('Pathloss(dB)');
 grid
%----------------------------------------------------
figure
hr1=0.5
htx=0.5
htx1=0.75
f=38:1.5:73
f=f.*10^9
db=(4*ht*hr1)./(c./f)
dby=(4*htx1*hr1)./(c./f)
dby1=(4*htx*hr1)./(c./f)
plot(f/1e9,db,'r-*','linewidth',1) ;hold on
plot(f/1e9,dby,'y-*','linewidth',1) ;hold on
plot(f/1e9,dby1,'k-*','linewidth',1) ;
xlabel('Frequecy (GHz)');
ylabel('Break point distance (m)');
legend('ht=1','ht=0.75','ht=0.5')
 grid
```